

DESIGN OF A LOW PROFILE CIRCULARLY POLARIZED PRINTED SLOT ANTENNA USING CSRR

A DISSERTATION

*Submitted in partial fulfillment of the
requirements for the award of the degree*

of

MASTER OF TECHNOLOGY

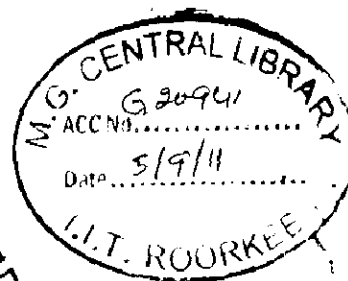
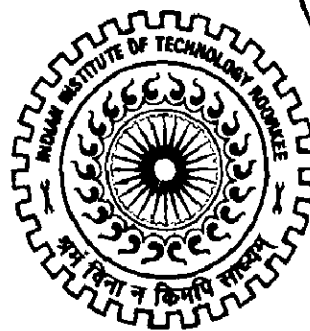
in

ELECTRONICS AND COMMUNICATION ENGINEERING

(With Specialization in RF & Microwave Engineering)

By

JAYESH UPADHYAY



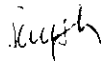
DEPARTMENT OF ELECTRONICS AND COMPUTER ENGINEERING
INDIAN INSTITUTE OF TECHNOLOGY ROORKEE
ROORKEE -247 667 (INDIA)
JUNE, 2011

Candidate's Declaration

I hereby declare that the work, which is being presented in the dissertation entitled, "**DESIGN OF A LOW PROFILE CIRCULARLY POLARIZED PRINTED SLOT ANTENNA USING CSRR**" which is submitted in the partial fulfillment of the requirements for the award of degree of **Master of Technology in RF & Microwave Engineering**, submitted in the Department of Electronics and Computer Engineering, **Indian Institute of Technology**, Roorkee (INDIA), is an authentic record of my own work carried out under the guidance of **Dr. S.N.SINHA**, HEAD OF DEPARTMENT, Department of Electronics and Computer Engineering, Indian Institute of Technology, Roorkee.

I have not submitted the matter embodied in this dissertation for the award of any other degree or diploma.

Date: __ June, 2011


(Jayesh Upadhyay)

Place: Roorkee


Enrol. No: 09533005

Supervisor's Certificate

This is to certify that this dissertation entitled, "**DESIGN OF A LOW PROFILE CIRCULARLY POLARIZED PRINTED SLOT ANTENNA USING CSRR**", which has been submitted by Jayesh Upadhyay is record of his own work carried out by him under my supervision. I also certify that the above statement made by the candidates is correct to the best of my knowledge and belief.

Date: __ June, 2011

Place: Roorkee


(Dr. S.N. SINHA)
Head Of Department
E&CE Department
IIT – Roorkee
Uttaranchal – 247667

Acknowledgement

It has been a great privilege of mine that I have got the opportunity to work with my advisor **Dr. S.N SINHA**, Head of the Department, Electronics and Computer Engineering, IIT Roorkee. I express my deepest gratitude to him for his valuable guidance, support and motivation in my work. I would like to thank him for his limitless interest and readiness to help me. The valuable discussion I had with him helped me a lot in putting my thoughts in right direction for attaining the desired objective.

I would also like to thank all the other respected professors for helping during the duration of the project.

I thank **Mr. Rajaram, Mr. SK Gaur and Mr. Giri** for their valuable support and time to time guidance in technical issues, which was instrumental in making this dissertation work a success. My gratitude to my parents whose support and unflinching encouragement has been a constant source of strength to me during the entire work.

JAYESH UPADHYAY

Enroll. No: 09533005

This dissertation reports the design of a low profile circularly polarized printed slot antenna using complementary split ring resonator (CSRR). The slot has the annular ring geometry and is fed by L shape feed line which couples the two orthogonal sides of the ring to provide circular polarization. The antenna is meant for the broad band application therefore a wide ring slot is used. The distinguishing feature of the design is that it incorporates the concept of single negative metamaterial for low profiling of the antenna. In this dissertation the frequency gap produced by an array of complementary split ring resonators (CSRRs) etched on the ground plane is also discussed. This behavior is interpreted as due to the presence of a negative effective dielectric permittivity in the vicinity of resonance. This behavior of CSRR is utilized in the design of the antenna.

Measured results show that antenna with CSRR reflector shows better performance than the antenna without CSRR reflector.

<i>Candidate's Declaration</i>	ii
<i>Acknowledgment</i>	iii
<i>Abstract</i>	iv
<i>Table of Contents</i>	v
<i>List of tables</i>	ix
<i>List of figures</i>	x
Chapter 1 Introduction	1
1.1 Literature and historical review	1
1.1.1 Aperture coupled microstrip patch antenna	1
1.1.2 Circularly polarized aperture coupled microstrip antenna	2
1.1.3 Complementary split ring resonators	5
1.2 Motivation	8
1.3 Statement of the problem	9
1.4 Organization of the dissertation	10
Chapter 2 Brief review of the work	11
2.1 Theory of aperture coupled microstrip antenna	12
2.1.1 Antenna substrate dielectric constant	12
2.1.2 Antenna substrate thickness	12
2.1.3 Microstrip patch length	12
2.1.4 Microstrip patch width	12
2.1.5 Feed substrate dielectric constant	12
2.1.6 Feed substrate thickness	12
2.1.7 Slot length	13
2.1.8 Slot width	13
2.1.9 Feed line width	13
2.1.10 Feed line position relative to slot	13
2.1.11 Position of the patch relative to the slot	13
2.1.12 Variations on the aperture coupled microstrip antenna	14

Table of Contents

	2.1.12.1	Variations on the aperture coupled microstrip antenna	14
	2.1.12.2	Slot shape	14
	2.1.12.3	Type of feed line	14
	2.1.12.4	Polarization	15
	2.1.12.5	Dielectric layers	15
	2.2	Theory of complementary split ring resonator	15
	2.2.1	Effective parameter extraction method	19
	2.2.2	CSRR as a reflecting surface	20
Chapter 3	Design of a circularly polarized antenna		23
	3.1	Design of annular ring slot circularly polarized antenna	23
	3.1.1	Antenna configuration	23
	3.1.2	Design procedure	25
	3.1.2.1	Variation of S11 (dB) and axial ratio (dB) with respect to l_p	26
	3.1.2.2	Variation of S11 (dB) and axial ratio (dB) with respect to w_s	27
	3.1.2.3	Variation of S11 (dB) and axial ratio (dB) with respect to d	28
	3.1.2.4	Variation of S11 (dB) and axial ratio (dB) with respect to l_s	30
	3.2	Simulated result of the optimized antenna	31
	3.2.1	S11 vs. Frequency	31
	3.2.2	Axial ratio vs. Frequency	32
	3.2.3	Gain vs. Frequency	33
	3.2.4	Discussion of simulated results	34
	3.3	Experimental setup	34
	3.4	Measured results	36

Table of Contents

3.4.1	Axial ratio vs. Frequency	37
3.4.2	S11 vs. frequency	37
3.4.3	Gain vs. Frequency	38
Chapter 4	Complementary split ring structure	40
4.1	Modeling of CSRR structure	41
4.1.1	Simulated results of CSRR with microstrip line	42
4.2	Effective electromagnetic parameters (ϵ_r) of CSRR structure with microstrip line	43
4.3	Equivalent circuit model of the CSRR structure	48
4.4	Measured permittivity and permeability	49
Chapter 5	Antenna with CSRR reflecting surface	52
5.1	Complementary split ring resonator as a reflecting surface	52
5.2	Simulated results of the antenna with reflector	53
5.2.1	S11 vs. Frequency	53
5.2.2	Axial ratio vs. Frequency	54
5.2.3	Radiation pattern	54
5.2.5	Discussion of measured results	56
Chapter 6	Conclusion and future scope	58
References		

Figures

Figure 1.1	Split ring resonator	7
Figure 1.2	Complementary split ring resonator	7
Figure 2.1	Aperture coupled microstrip antenna	11
Figure 2.2	Layout of CSRR-loaded microstrip	17
Figure 2.3	Equivalent circuit of CSRR-loaded microstrip	18
Figure 2.4	Magnitude of S parameters	18
Figure 2.5	Phase of S parameters	19
Figure 2.6	Constructive interference of transmitted and reflected wave when reflecting plane is at $\lambda/4$ away from antenna	22
Figure 3.1	Antenna configuration	24
Figure 3.2	Variation of (a) axial ratio and (b) S11 with l_p	26
Figure 3.3	Variation of (a) axial ratio and (b) S11 with w_p	28
Figure 3.4	Variation of (a) axial ratio and (b) S11 with d	29
Figure 3.5	Variation of S11 and axial ratio with l_s	30
Figure 3.6	S11 vs. Frequency	31
Figure 3.7	Axial ratio vs. Frequency	32
Figure 3.8	Gain vs. Frequency	33
Figure 3.9	Measuring set up for S11	34
Figure 3.10	Set up for the measurement of axial ratio and gain	35
Figure 3.11	Axial ratio vs. Frequency	36
Figure 3.12	S11 vs. Frequency	37
Figure 3.13	Gain vs. Frequency	38
Figure 4.1	Top view	40
Figure 4.2	Bottom view	40
Figure 4.3	Single unit CSRR structure	41
Figure 4.4	S11 (dB) vs. Frequency	42
Figure 4.5	S21 (dB) vs. frequency	43
Figure 4.6	Real epsilon vs. Frequency	44
Figure 4.7	Imaginary epsilon vs. frequency	45
Figure 4.9	Imaginary μ vs. Frequency	47

List Of Figures

Figure 4.10	Equivalent circuit model of microstrip loaded with CSRR structure	49
Figure 4.11	Complex permittivity vs. Frequency	50
Figure 4.12	Complex permeability vs. Frequency	51
Figure 5.1	CSRR reflector	52
Figure 5.2	Reflector h distance below the antenna	53
Figure 5.3	S11 vs. frequency	53
Figure 5.4	Axial ratio vs. frequency	54
Figure 5.5	Radiation pattern	55
Figure 5.6	S11 Vs Frequency	56
Figure 5.7	Axial ratio (dB) Vs Frequency	57
Figure 5.8	Radiation pattern	57

List of Tables

Table 3.1	Initial geometric parameters of antenna	26
Table 3.2	Geometrical parameters of optimized antenna	31
Table 3.3	Gain vs. Frequency	38
Table 4.1	Geometrical parameters of a single CSRR structure	41
Table 4.2	Variation of real epsilon with frequency	44
Table 4.3	Variation of Imag (ϵ_p) with frequency	45
Table 4.4	Variation of Real (μ) with frequency	46
Table 4.5	Variation of Imag (μ) with frequency	47
Table 4.6	Parameters and values of equivalent circuit of CSRR with microstrip line	49

CHAPTER 1

Introduction

1.1 Literature and historical review

1.1.1 Aperture coupled microstrip patch antenna

An antenna is a transitional device between two medium, generally a free space and a guiding device. The guiding device can be a coaxial line or a hollow wave guide. In other words an antenna is a transducer that converts electromagnetic waves into voltages (or current) and vice versa. For wireless communication the antenna is of paramount importance, where it is used for transmitting and receiving. Over the years wireless technology has developed manifolds, this necessitates the development of a good design of antenna which can meet the requirement of any wireless system. For example in its early years an antenna was just a probing device but as the years went by those antennas were developed which could optimize or accentuate the radiation energy in some direction and suppress in others. These days aperture coupled printed slot antennas have attracted much attention due to their smaller size and being highly efficient in higher frequency. The first aperture coupled microstrip antenna was successfully designed and fabricated in 1984, by this time basic microstrip antenna was well establish in terms of design and modelling and people were searching for new ways to develop a high performance microstrip antenna, specifically they were trying to increase the bandwidth. One of these applications involved the use of microstrip antennas for integrated phased array systems, as the printed technology of microstrip antenna seemed perfectly suited to low-cost and high-density integration with active MIC or MMIC phase shifter and T/R circuitry. One group at the University of Massachusetts (Dan Schaubert, Bob Jackson, Sigfrid Yngvesson, and D.M Pozar) had received an Air Force contract to study this problem. Their approach of building an integrated millimeter wave array (or sub array) using a single GaAs substrate layer had several drawbacks.

First, there is generally not enough space on a single layer to hold antenna elements, active phase shifter and amplifier circuitry, bias lines, and RF feed lines.

Second, the high permittivity of a semiconductor substrate such as GaAs was a poor choice for antenna bandwidth, since the bandwidth of a microstrip antenna is best for low dielectric constant substrates. And if substrate thickness is increased in an attempt to improve bandwidth, spurious feed radiation increases and surface wave power increases. This latter problem ultimately leads to scan blindness, whereby the antenna is unable to receive or transmit at a particular scan angle. One obvious possibility was to use two back-to-back substrates with feed through pins. This would allow plenty of surface area, and had the critical advantage of allowing the use of GaAs (or similar) material for one substrate, with a low dielectric constant for the antenna elements. The main problem with this approach was that the large number of via holes presented fabrication problems in terms of yield and reliability. Finally they arrived at an idea of using a slot or aperture to couple a microstrip feed line to a resonant microstrip patch antenna. After considering the application of small hole coupling theory to the fields of the microstrip line and the microstrip antenna, they designed a prototype element for testing. Their theory was very simple, but good enough to suggest that maximum coupling would occur when the feed line was centered across the aperture, with the aperture positioned below the center of the patch, and oriented to excite the magnetic field of the patch. The first aperture coupled microstrip antenna was fabricated and tested by a graduate student, Allen Buck, on August 1, 1984, in the University of Massachusetts Antenna Lab. This antenna used 0.062" Duroid substrates with a circular coupling aperture, and operated at 2 GHz.

1.1.2 Circularly polarized aperture coupled microstrip antenna

As wireless technology is growing, more stringent constraints are imposed upon the mobile system. With antenna in particular these constraints are more serious as antenna is the front end of the system. There are various problems faced by mobile wireless designer. Circularly polarized antenna is better equipped for these problems than linearly polarized antenna. Some problems generally faced by a mobile wireless system designer are given below

Reflectivity: Radio signals are reflected or absorbed depending on the material they come in contact with. Because linearly polarized antennas are able to receive maximum signal only if plane of polarization of the incident wave matches with that of the antenna, if the reflecting surface does not reflect the signal precisely in the same plane, a part of the signal strength will be lost. Since circularly polarized antennas send and receive in all planes, the signal strength is not lost, but is transferred to a different plane and is still utilized.

Absorption: As stated above, radio signal can be absorbed depending on the material they come in contact with. Different materials absorb the signal from different planes. As a result, circular polarized antennas give you a higher probability of a successful link because it is transmitting on all planes.

Phasing Issues: High-frequency systems (i.e. 2.4 GHz and higher) that use linear polarization typically require a clear line-of sight path between the two points in order to operate effectively. Such systems have difficulty penetrating obstructions due to reflected signals, which weaken the propagating signal. Reflected linear signals return to the propagating antenna in the opposite phase, thereby weakening the propagating signal. Conversely, circularly-polarized systems also incur reflected signals, but the reflected signal is returned in the opposite orientation, largely avoiding conflict with the propagating signal. The result is that circularly-polarized signals are much better at penetrating and bending around obstructions.

Multi-path: Multi-path is caused when the primary signal and the reflected signal reach a receiver at nearly the same time. This creates an "out of phase" problem. The receiving radio must spend its resources to distinguish, sort out, and process the proper signal, thus degrading performance and speed. Linear Polarized antennas are more susceptible to multi-path due to increased possibility of reflection. Out of phase radios can cause dead-spots, decreased throughput, distance issues and reduce overall performance in a 2.4 GHz system.

Inclement Weather: Rain and snow causes a microcosm of conditions explained above (i.e. reflectivity, absorption, phasing, multi-path and line of sight) Circular polarization is more

resistant to signal degradation due to inclement weather conditions for all the reason stated above.

Line-of-Sight: When a line-of-sight path is impaired by light obstructions (i.e. foliage or small buildings), circular polarization is much more effective than linear polarization for establishing and maintaining communication links.

Traditional microstrip patch antennas can provide CP with good gain performance but they suffer from the problem of limited impedance and axial-ratio bandwidths. An alternative can be the use of printed slot antennas which provide a wider bandwidth as compared to their patch antennas [1-3].

Ring structure can reduce the antenna size by the factor of 2 when compared to the conventional linear printed slot antennas. CP radiation in the ring structures is achieved by introducing some symmetric or asymmetric perturbation of the slot. In [4], a 3-dB axial ratio CP bandwidth of 3-4% was achieved for a singly-fed slot ring antenna. Further improvement of CP bandwidth in slot antennas came with the use of coplanar waveguide feeds. An 18% 3-dB axial ratio bandwidth was reported in [5], where a wide square slot antenna was fed by a coplanar waveguide. Another method to improve bandwidth is the use of hybrid coupler to provide the 90° phase over a wide frequency band. The annular and square ring antennas using this hybrid provided CP bandwidths of 9% and 22% respectively [6, 7]. However, the use of hybrids requires a larger area and also, additional transmission losses occur in these hybrids. In [8], a narrow square-ring slot antenna with an L-shaped series feed configuration was proposed. Although a gain of 3.5 dBic and an impedance bandwidth of 15% were achieved, good CP performance was obtained only over a 6% bandwidth, thus limiting the usable bandwidth to 6%.

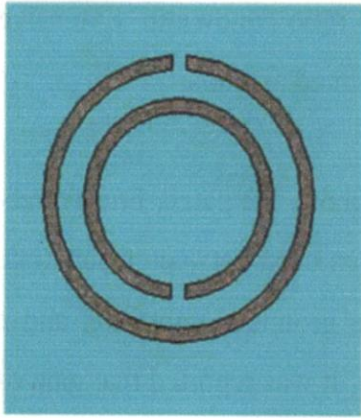
1.1.3 Complementary split ring resonators

In last few years, there has been an extensive research effort within the electromagnetic community to develop and use novel metamaterials (i.e. artificially fabricated materials, based on periodic structures, with properties not existing in nature). Among these materials, electromagnetic bandgap (EBG) structures, negative- μ , negative- ϵ , and left-handed (LH) media have received much attention in the microwave engineering [9]. One interesting application proposed for these structures has been the filtering of frequency bands and/or the suppression of undesired spurious pass bands or harmonics in microwave circuits. Traditional techniques are based on the use of half wavelength short circuit stubs, chip capacitors or cascaded rejection band filters, but they are narrow band, high profile and very lossy and this degrades circuit performance. These drawbacks have been minimized by the introduction of the Bragg-effect-related Electromagnetic Band Gap(EBG) concept. EBG devices obtained by etching holes or patterns in the ground plane and it observed that they exhibit wide and deep stop bands [10]. This technique has been successfully used to achieve broad-band harmonic tuning in power amplifiers, oscillators and mixers; to increase output power and efficiency and to reduce spurious harmonic content. The implementation of lowpass filters with huge rejection bandwidth and the implementation of microstrip bandpass filters with spurious passband suppression have been also demonstrated [11]. Usually, in all cited applications, EBG structures are integrated within the device and no extra circuit area is required. However, EBG's scale with frequency, require several periods to provide significant rejection and, therefore, can be relatively large for certain frequency band applications. This problem has been recognized and addressed in [12]. The novel compact EBG structures proposed there produce a high rejection and wide stopband with small length. Nevertheless the transversal dimension of the structure is still large (at the cutoff frequency) since it is based on resonating transversal slots. Moreover, the uniform (potentially more compact) configuration exhibits significant radiation at the stopband. Recently, negative- and LH structures have appeared as an alternative to EBGs for tailoring the frequency response of microwave devices. As it was theoretically and experimentally demonstrated in [13] a three dimensional periodic structure formed by an array of split ring resonators (SRRs) excited by a properly polarized radiation (i.e., magnetic field parallel to ring axis) is able to inhibit signal propagation in the vicinity of the resonant frequency. This can be interpreted as due to the

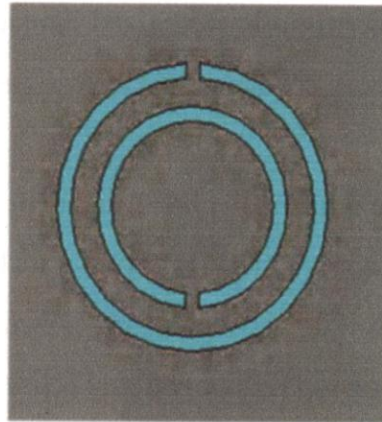
properties of the periodic medium, which exhibits a high negative effective magnetic permeability in a narrow frequency range around and above the resonance frequency. Actually the SRR proposed in [13] as a basic particle for the design of artificial negative magnetic permeability media, and it became very popular because it was used in the first physical realization of an LH medium [14]. It is important to note that the inhibition of signal propagation achieved in the above mentioned periodic structure is not due to Bragg-like diffraction, but to the behavior of the constituent particles. Therefore, the period of the structure can be much smaller than the wavelength, in contrast to the case of conventional EBGs. These remarkable properties, together with its planar nature, make the SRR a very interesting particle to implement compact structures in microstrip or CPW technology. In fact, the possibility of designing stopband negative- structures using SRRs has been recently demonstrated [15]. SRR structure was originally proposed by Pendry *et al.* [13] which are small resonant particles with a high quality factor at microwave frequencies. When they are excited by an external time varying magnetic field applied parallel to the ring axis, an electromotive force around the rings is generated giving rise to current loops in the rings. These current loops are closed through the distributed capacitance between the concentric rings. According to this, the SRR behaves as an externally driven LC circuit with a resonant frequency that can be easily tuned by varying device dimensions. By invoking the concepts of duality and complementarity the Complementary Split Ring Resonator (CSRR) can be derived from the SRR structure in a straightforward way. This new particle, which in planar technology can be defined as the *negative* of the SRR, exhibits an electromagnetic behavior which is almost the *dual* of that of the SRR. Specifically, a negative-ε effective permittivity can be expected for any CSRR-based medium, whereas a negative-ε behavior arises in an equivalent SRRs system. In contrast to the usual transmission line resonators, CSRRs are sub-lambda structures, i.e., their dimensions are electrically small at the resonant frequency (typically one tenth of the guided wavelength or less). Therefore, high level of miniaturization is expected by using these particles.

Moreover, the CSRR structure [Fig 1.2] has the advantage over other SRR [Fig 1.1] designs of an easier implementation in microstrip technology. In fact, coupling between CSRRs and the line can be simply achieved by etching the CSRRs in the ground plane, whereas magnetic coupling

between the line and SRRs needs additional metallizations in the strip plane [16], which substantially increases transversal dimensions.



Split ring resonator
Fig 1.1



Complementary split ring resonator
Fig 1.2

1.2 Motivation

Circularly polarized printed slot antennas are extensively researched, but like every printed slot antenna they suffer from low gain and limited impedance and axial ratio bandwidth. Extensive researches have been conducted to increase gain and bandwidth of printed antenna.

In a resonance gain method [17-19], layers of dielectric are stacked above the patch. For a three-layer electromagnetically (EM) coupled structure; an air layer is often used between a substrate and a superstrate [20, 21]. The patch is etched on top surface of a grounded substrate, and a coupled patch is on top [20] or bottom [21] surface of the superstrate. It was reported that gain of the patch antenna can be increased by tuning thickness of the air layer. In [20], the spacing is between 0.31, and 0.37. In [21], the spacing is approximately one half free space wavelengths.

Some authors used a PEC reflector in apertures coupled slot antenna, the PEC reflector makes the antenna unidirectional, thus increasing the gain of antenna, but the major disadvantage of this method is that it makes the antenna a high profile antenna, as the reflector must be kept at at least $\lambda/4$ below the antenna.

In [22] the authors used a radome etched with CSRR on both sides instead of patch [23], but despite of using CSRR the bandwidth suffered as attempts are made to make it a low profile.

Thus design of a low profile, high gain broadband circularly polarized antenna antenna remains a challenge.

1.3 Statement of the problem

The problem undertaken in this dissertation is to design a low profile, circularly polarized, printed slot antenna and verify its performance experimentally.

The problem can be sub divided into following parts

1. Design of a circularly polarized aperture coupled printed slot antenna
2. Design of a CSRR structure whose stop band characteristics falls in the operating frequency region of above mentioned antenna.
3. Combining the two designs to get desired results in the operating frequency region.

1.4 Organization of the dissertation

The theoretical background required for circularly polarized aperture coupled antenna and complement split ring resonator is presented in chapter 2. The theory includes some basic features of slot antenna and CSRR structures. Simulation and experimental results of antenna are presented in chapter 3. Simulated results of antenna include variation of VSWR, reflection coefficient, axial ratio, gain with frequency whereas simulated results of CSRR include two port parameters S_{11} and S_{21} , variation of μ and ϵ with frequency. Chapter 4 includes the Simulation and experimental results of antenna with CSRR as a reflecting surface. Experimental results include reflection coefficient, axial ratio and gain measurement for antenna; measurement variation of μ and ϵ for CSRR. Chapter 5 contains simulated and experimental results of antenna with CSSR reflecting surface.

CHAPTER 2

Brief review of the work

2.1 Theory of aperture coupled microstrip patch antenna

Figure 2.1 shows the geometry of the basic aperture coupled microstrip antenna. The radiating microstrip patch element is etched on the top of the antenna substrate, and the microstrip feed line is etched on the bottom of the feed substrate. The thickness and dielectric constants of these two substrates may thus be chosen independently to optimize the distinct electrical functions of radiation and circuitry.

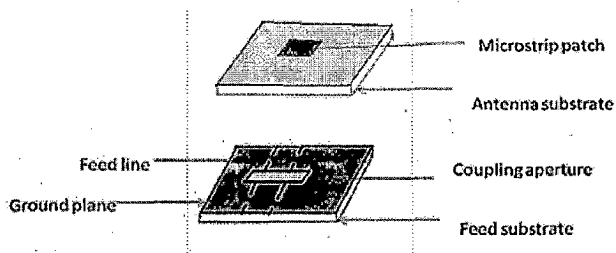


Figure 2.1 Aperture coupled microstrip antenna

The aperture coupled microstrip antenna involves over a dozen material and dimensional parameters, and summarized below the basic effects of these parameters on the radiation characteristics of these antennas:

2.1.1 Antenna substrate dielectric constant:

This primarily affects the bandwidth and radiation efficiency of the antenna, with lower permittivity giving wider impedance bandwidth and reduced surface wave excitation.

2.1.2 Antenna substrate thickness:

Thickening the substrate increases the operational bandwidth, but at the same time increases the excitation of substrate surface modes and a trade-off must be performed

2.1.3 Microstrip patch length:

The length of the patch radiator determines the resonant frequency of the antenna.

2.1.4 Microstrip patch width:

The width of the patch affects the resonant resistance of the antenna, with a wider patch giving a lower resistance. Square patches may result in the generation of high cross polarization levels, and thus should be avoided unless dual or circular polarization is required.

2.1.5 Feed substrate dielectric constant:

This should be selected for good microstrip circuit qualities, typically in the range of 2 to 10.

2.1.6 Feed substrate thickness:

Thinner microstrip substrates result in less spurious radiation from feed lines, but higher loss. A compromise of 0.01λ to 0.02λ is usually good.

2.1.7 Slot length:

The length of the coupling slot, determines the coupling level as well as the back radiation level. The slot should therefore be made no larger than is required for impedance matching.

2.1.8 Slot width:

The width of the slot also affects the coupling level, but to a much less degree than the slot width. The ratio of slot length to width is typically 1/10 to keep the cross polarization at a low level.

2.1.9 Feed line width:

Besides controlling the characteristic impedance of the feed line, the width of the feed line affects the coupling to the slot. To a certain degree, thinner feed lines couple more strongly to the slot.

2.1.10 Feed line position relative to slot:

For maximum coupling, the feed line should be positioned at right angles to the center of the slot. Skewing the feed line from the slot will reduce the coupling, as will positioning the feed line towards the edge of the slot.

2.1.11 Position of the patch relative to the slot:

For maximum coupling, the patch should be centered over the slot. Moving the patch relative to the slot in the H-plane direction has little effect, while moving the patch relative to the slot in the E-plane (resonant) direction will decrease the coupling level.

2.1.12 Variations on the aperture coupled microstrip antenna:

Since the first aperture coupled microstrip antenna was proposed, a large number of variations in geometry have been suggested by workers around the world. The fact that the aperture coupled antenna geometry lends itself so well to such modifications is due in part to the nature of printed antenna technology itself, but also to the multi-layer structure of the antenna. Below we categorize some of the modified designs that have evolved from the basic aperture coupled antenna geometry:

2.1.12.1 Variations on the aperture coupled microstrip antenna:

The original aperture coupled antenna used a single rectangular patch. Since then, workers have successfully demonstrated the use of circular patches, stacked patches, parasitically coupled patches, patches with loading slots, and radiating elements consisting of multiple thin printed dipoles. Most of these modifications are intended to yield improved bandwidth.

2.1.12.2 Slot shape:

The shape of the coupling aperture has a significant impact on the strength of coupling between the feed line and patch. Thin rectangular coupling slots have been used in the majority of aperture coupled microstrip antennas, as these give better coupling than round apertures. Slots such as annular slots, cross slots, "dogbone", bow-tie, or H-shaped apertures can further improve coupling.

2.1.12.3 Type of feed line:

The microstrip feed line can be replaced with other planar lines, such as stripline, coplanar waveguide, dielectric waveguide, and similar lines. The coupling level may be reduced with such lines, however. It is also possible to invert the feed substrate, inserting an additional dielectric layer so that the feed line is between the ground plane and the patch element.

2.1.12.4 Polarization:

Besides linear polarization, it has been demonstrated that dual polarization and circular polarization can be obtained with aperture coupled elements. In [23], in order to obtain circular polarization cross slot is used with an L shaped microstrip line.

2.1.12.5 Dielectric layers: As with other types of microstrip antennas, it is easy to add a radome layer to an aperture coupled antenna, either directly over the radiating element, or spaced above the element. It is also possible to form the antenna and feed substrates from multiple layers, such as foam with thin dielectric skins for the etched conductors.

2.2 Theory of complementary split ring resonator

It is well known, the complementary of a planar metallic structure is obtained by replacing the metal parts of the original structure with apertures, and the apertures with metal plates. It is known that if the thickness of the metal plate is zero, and its conductivity is infinite (perfect electric conductor), then the apertures behave as perfect magnetic conductors. In that case the original structure and its complement are effectively dual and if the field $F(E, H)$ is a solution for the original structure, its dual $F'(E', H') = (-\sqrt{\mu/\epsilon} \cdot H, \sqrt{\mu/\epsilon} \cdot E)$ is the solution for the complementary structure. A CSRR can be implemented in microstrip technology by etching the rings in the ground plane, just underneath the conductor strip. This arrangement ensures that CSRR are properly excited by an electric field polarized in the axial direction of the ring. It is important to note that the so obtained CSRR is not the exact dual of the conventional SRR. This is due to the presence of the dielectric slab which introduces an additional boundary condition at a distance of the SRR plane. However they will be approximately dual and the behavior of the complementary structure excited by an axial electric field will be similar to that of the original.

Since the roles are changed in the CSRR and the SRR due to duality at resonant frequency a strong and resonant electric dipole should appear in the CSRR, which is the dual of the strong magnetic polarizability appearing in the SRR. Therefore, a region of very high and consecutive positive and negative electric polarizability is expected around this frequency [24]

The basic structure under study is a CSRR-loaded microstrip line [fig 2.2]. The microstrip line serves as the host medium and it consists of a substrate with a conducting strip on the top side and a conducting plane (ground plane) on the bottom side. The CSRRs are etched in the ground plane just below the conducting strip. The dominant mode in the microstrip line is the quasi-TEM mode and it can be excited by feeding the ports. For the quasi-TEM mode, the electrical field polarization is basically perpendicular to the ground plane, especially in the region between the conducting strip and the ground plane. Hence, the electrical field is parallel to the axis of the CSRR and this satisfies the requirement for generating negative permittivity. As long as the size of the CSRR is electrically small, the structure can be described by means of lumped elements. The equivalent circuit model is shown in figure 2.3. This model consists of a three-element LC tank circuit embedded between two segments of microstrip lines. The shunt LC tank circuit includes a series LC resonator (L and C_1) and a capacitance element (C_2) connected in parallel. The reference planes of the input and the output ports are chosen to lie at the edges of the CSRR, which are indicated as T1 and T2 in figure 2.3. The length of the microstrip line d in the equivalent circuit can be obtained by fitting the phase of the scattering parameters. In view of the model, two characteristic frequencies f_1 and f_2 [fig 2.4] can be identified: f_1 is given by the resonance condition of the whole tank circuit, which leads to the zeros of the reflection coefficient (S_{11}). f_2 is given by the resonance condition of the series LC circuits (L and C_1), which leads to the zeros of the transmission coefficient (S_{21}). These frequencies are given by the following expressions:

$$f_1 = \frac{1}{2\pi} \sqrt{\frac{C_1 + C_2}{LC_1 C_2}} \quad (2.1)$$

$$f_2 = \frac{1}{2\pi} \sqrt{\frac{1}{LC_1}} \quad (2.2)$$

They can be easily determined by simulation or experiment. To determine the three lumped elements in the equivalent circuit, an additional equation is necessary. Here, we choose the third characteristic frequency f_3 by forcing the insertion loss to be 3 dB:

$$20 \log [S_{21}|_{f_3}] = -3 \text{ dB} \quad (2.3)$$

Under lossless condition, f_3 is the intersection of S_{11} and S_{21} , as shown in figure 2.4. Based on equations (2.1)–(2.3), we can determine the lumped elements. The detailed expressions are as follows:

$$c_2 = \frac{Y_0(f_2^2 - f_1^2)}{\pi f_2(f_1^2 - f_2^2)} \quad (2.4)$$

$$c_1 = \left(\frac{f_1^2}{f_2^2} - 1 \right) c_2 \quad (2.5)$$

$$L = \frac{1}{4\pi^2 f_2^2 c_1} \quad (2.6)$$

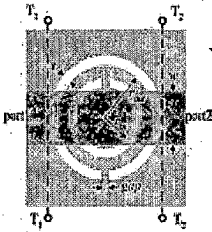


Figure 2.2 Layout of CSRR-loaded microstrip[24]

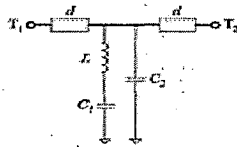


Figure 2.3 Equivalent circuit of CSRR-loaded microstrip[24]

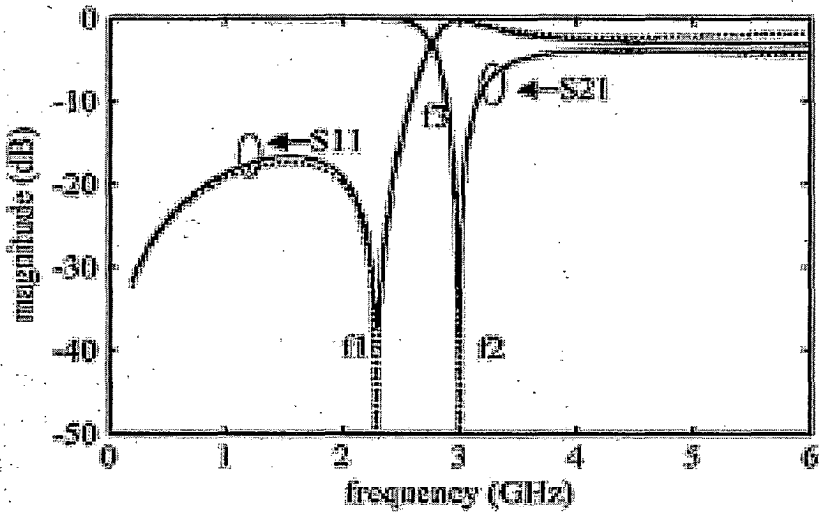


Figure 2.4 Magnitude of S parameters [24]

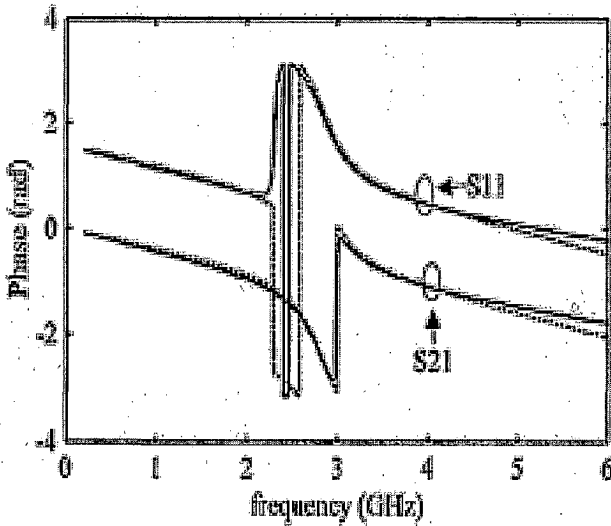


Figure 2.5 Phase of S parameters[24]

2.2.1 Effective parameter extraction method [25]

To observe the variation of permittivity and permeability with frequency there are many methods. The method used in this thesis is Nicolson-Ross-Weir (NRW) approach [25]. S parameters (reflection (S11), transmission (S21)) are obtained by arrangement shown in figure 2.2

$$\tau = k \mp \sqrt{k^2 - 1} \quad (2.6)$$

$$k = \frac{s_{11}^2 - s_{21}^2 + 1}{2s_{11}} \quad (2.7)$$

\mp is chosen so that $|\tau| < 1$

$$Z_{\text{eff}} = [(1+\tau)/(1-\tau)]/\sqrt{\epsilon_r} \quad (2.8)$$

$$\gamma = \mp \frac{\cosh^{-1} \left(\frac{s_{11}^2 - s_{21}^2 + 1}{2s_{11}} \right)}{L} \quad (2.9)$$

$$\eta = \sqrt{\mu_{eff} \epsilon_{eff}} \quad (2.10)$$

$$= \mp \frac{1}{jL} \left(\frac{C}{\omega} \right) \cosh^{-1} \left(\frac{\sqrt{\epsilon_{11} - \epsilon_{22}} + 1}{2\epsilon_{22}} \right) \quad (2.11)$$

\mp is chosen so that $\text{imag}(\eta) < 0$

$$\mu_{eff} = \eta \cdot Z_{eff} \quad (2.12)$$

$$\epsilon_{eff} = \eta / Z_{eff} \quad (2.13)$$

2.2.2 CSRR as a reflecting surface

An important property of metals is that they support surface waves. These are propagating electromagnetic waves that are bound to the interface between metal and free space. They are called surface plasmons at optical frequencies, but at microwave frequencies, they are nothing more than the normal AC currents that occur on any electric conductor. If the conductor is smooth and flat, the surface waves will not couple to external plane waves. However, they will radiate if scattered by bends, discontinuities, or surface texture. Bound surface waves do not exist on an ideal "perfect electric conductor" since, in the limit of infinite conductivity; the fields associated with surface currents extend to an infinite distance into space.

Surface waves appear in many situations involving antennas. If an antenna is placed near a metal sheet, such as a reflector or ground plane, it will radiate plane waves into free space, but it will also generate currents that propagate along the sheet. On an infinitely large ground plane, the surface currents would not affect the radiation pattern of antenna but there will be a slight decrease in the radiation efficiency. Practically the ground plane is always of finite size, and

these currents propagate until they reach an edge or corner. Any discontinuity surface allows the currents to radiate; these radiated waves will interfere with the radiation pattern of antenna and distort it.

While a conductive surface is a good reflector, it has the unfortunate property of reversing the phase of reflected waves. Good conductors have zero tangential electric field at the surface. When an electromagnetic wave impinges on a conductor, the reflected wave experiences a phase reversal to ensure that the tangential electric field is zero at the surface. Likewise, the magnetic field has antinodes at the surface. Unfortunately, if the antenna is too close to the conductive surface, the phase of the impinging wave is reversed upon reflection, resulting in destructive interference with the wave emitted in the other direction by the antenna. This problem is solved by including a one-quarter wavelength space between the radiating element and the ground plane, as shown in Figure 2.5. The total round trip phase shift from the antenna, to the surface, and back to the antenna, equals one complete cycle, and the waves add constructively. The antenna radiates efficiently, but the entire structure requires a minimum thickness of $\lambda/4$.

Keeping a conducting reflecting surface at $\lambda/4$ will theoretically increase the gain by 3 dB but this increases the antenna a high profile to $\lambda/4$ which can be quite large at lower RF frequency, also the unwanted radiation from the edges of the reflector will distort the radiation pattern of the antenna.

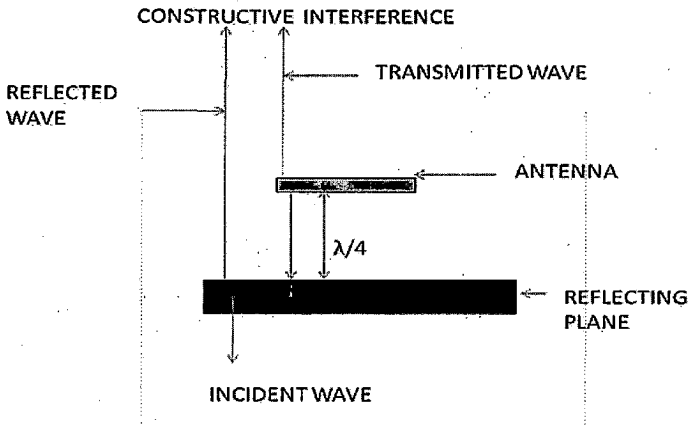


Figure 2.6 Constructive interference of transmitted and reflected wave when reflecting plane is at $\lambda/4$ away from antenna

The above mentioned problem can be ameliorated by etching CSRR rings on the reflecting surface. CSRR has the band stop property, which will prohibit the propagation of surface waves (current) and it will not reverse the phase of the reflected wave, a CSRR can be modeled so that the phase of the reflected wave is same as that of the incident wave, which means a conductive reflecting surface with CSRR ring etched on it can be placed quite close to the antenna.

CHAPTER 3

Design of a circularly polarized antenna

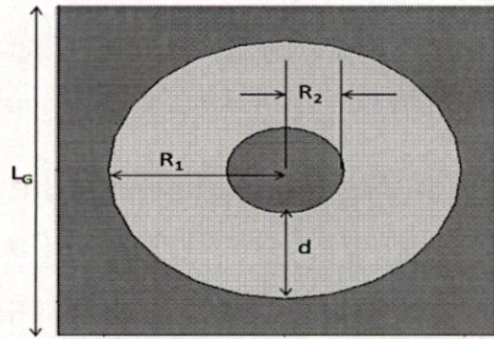
This chapter of the thesis deals with the design of circularly polarized annular ring slot antenna and simulation and experimental investigation of this antenna. Simulated results include return loss (S11) vs. frequency, axial ratio vs. frequency and gain vs. frequency. Measured results include return loss (S11) vs. frequency, axial ratio vs. frequency, gain vs. frequency and radiation pattern.

3.1 Design of annular ring slot circularly polarized antenna

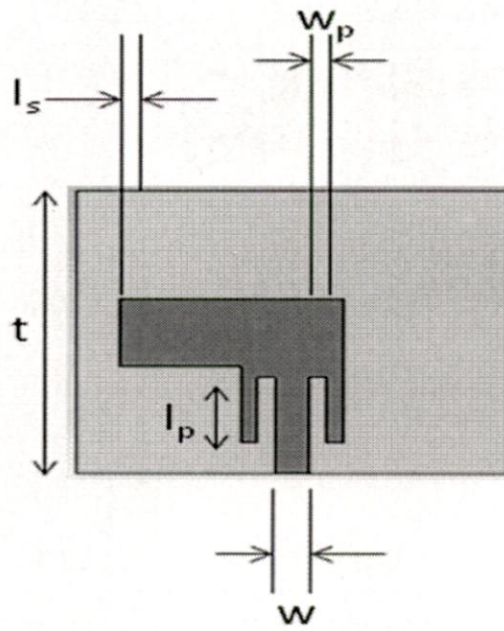
3.1.1 Antenna configuration

The geometry of the proposed antenna is shown in Figure 3.1. The substrate has an annular ring slot on its top surface. The annular slot is fed by an L-strip of width t , which couples to the two orthogonal sides of the ring. At one end, the extension of L strip beyond the slot (l_s) acts as an open circuited stub and at the other end, the L strip has slots of length l_p and width w_p cut on it. The outer radius of the annular ring is R_1 and inner radius is R_2 . The ground is of square shape and the length of one side is L_G . The 50 ohm microstrip line has width w . The L shape strip line has width d . All these parameters are to be fine tuned for CP operation and matching.

In fig 3.1 the orientation of the L-arm gives Right Hand Circular Polarization (RHCP), if the orientation of L arm is reversed Left Hand Circular Polarization (LHCP) is obtained.



(a) Top view



(b) Bottom view

Figure 3.1 Antenna configuration

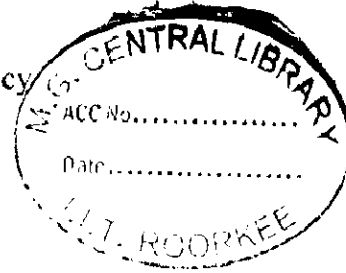
3.1.2 Design procedure

At operating frequency, the circumference of the slot ring is of the order of one wave length. Since the slot is at the interface between dielectric and the air, the effective wavelength here is taken as the average of free space wave length and the guided wavelength in the dielectric

$$\lambda_{eff} = \frac{\lambda_c + \lambda_d}{2} \quad (3.1)$$

λ_c is the free space wavelength at operating frequency

λ_d is the guided wavelength in the dielectric



The median of the circumference of the outer and the inner radius corresponds to the effective wavelength (λ_{eff}) at operating frequency.

$$2\pi \left(\frac{R_1 + R_2}{2} \right) = \lambda_{eff} \quad (3.2)$$

Since the antenna is meant for the broad band application; therefore a wide ring slot is required [26]. The initial value slot width ($R_1 - R_2$) is taken as $0.17\lambda_{eff}$. Wide ring slot leads to mismatch, to rectify this problem slots of length l_p and width w_p are cut in the L shape feed line. Initially l_p and w_p are kept zero.

The width of the strip line t is taken $0.08\lambda_{eff}$

The initial size of the ground is taken as $L_G = \frac{\lambda_{eff}}{2}$.

w is the width of 50 ohm microstrip line on the substrate of dielectric constant 3.34

Table 3.1 Initial geometric parameters of antenna

Parameter	L_G	R_1	R_2	w_p	l_s	l_p	w	d	t
Dimension(mm)	50	22	4.5	0	0	0	4	17.5	10

3.1.2.1 Variation of S11 (dB) and axial ratio (dB) with respect to l_p

Using a wide slot will lead to the mismatch resulting in poor return loss, to improve the problem, slots are cut on the feed line. l_p is varied from 0mm to 15mm with $w_p=1$ mm while keeping the other parameters to their initial values. Variation of S11 and axial ratio with l_p is shown Figure 3.2. It is observed that when $l_p = 0$ mm, axial ratio is satisfactory (less than 3(dB)) but return loss is very poor. As l_p is increased to 7.5mm S11 is improved a little but axial ratio deteriorates, so l_p is further increased. When l_p is increased to 15mm axial ratio and S11 improved significantly.

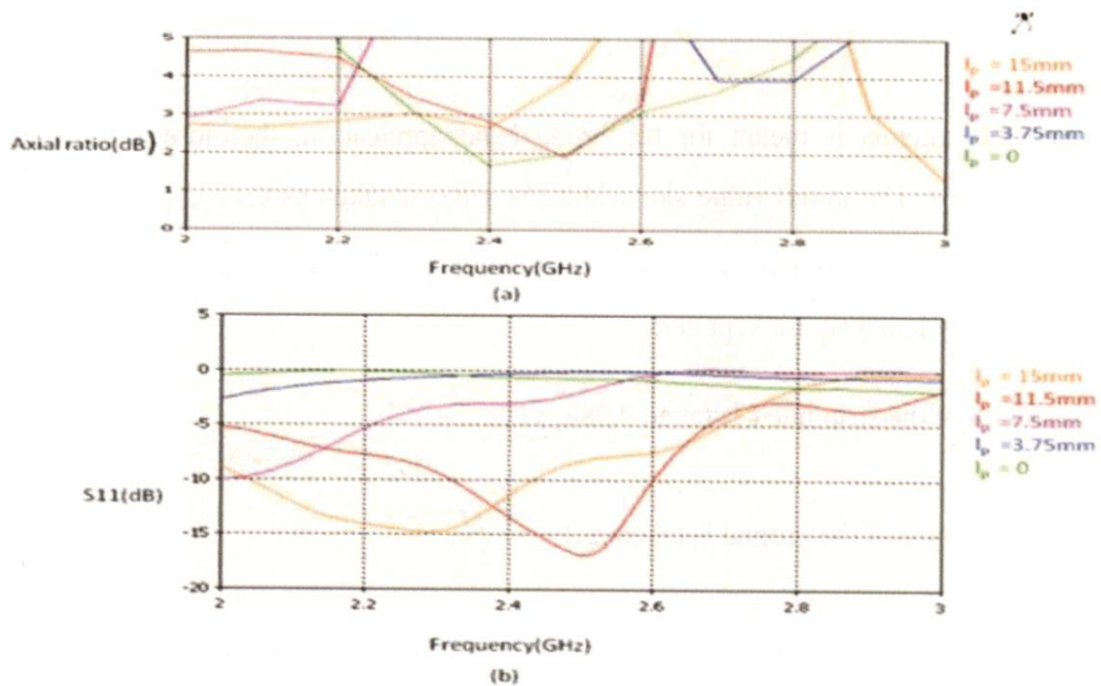
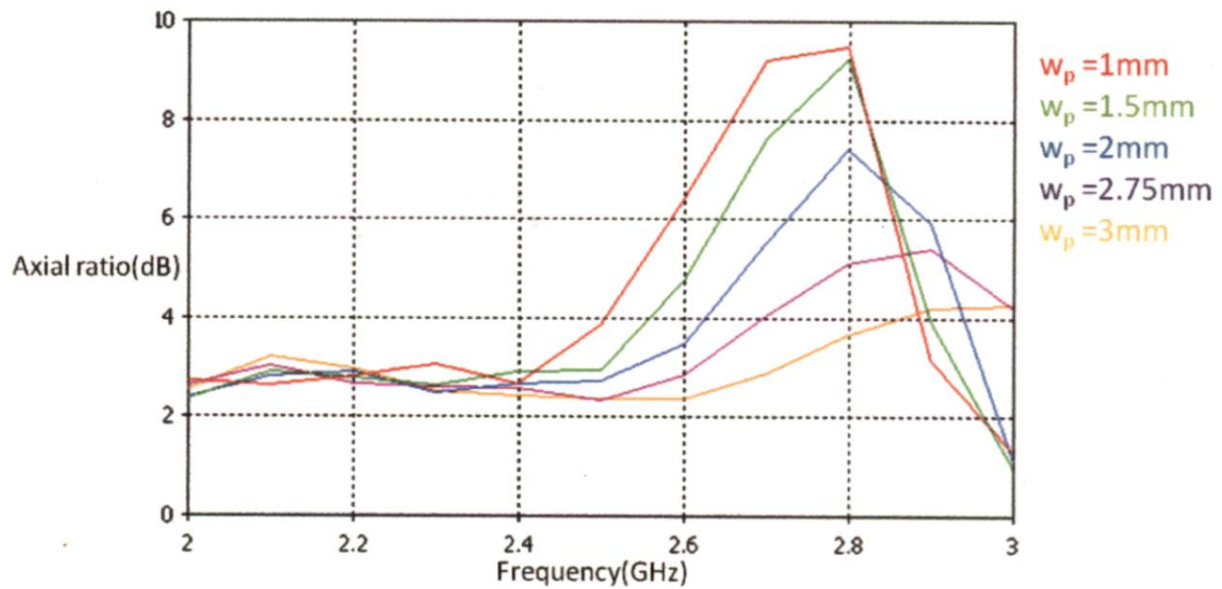


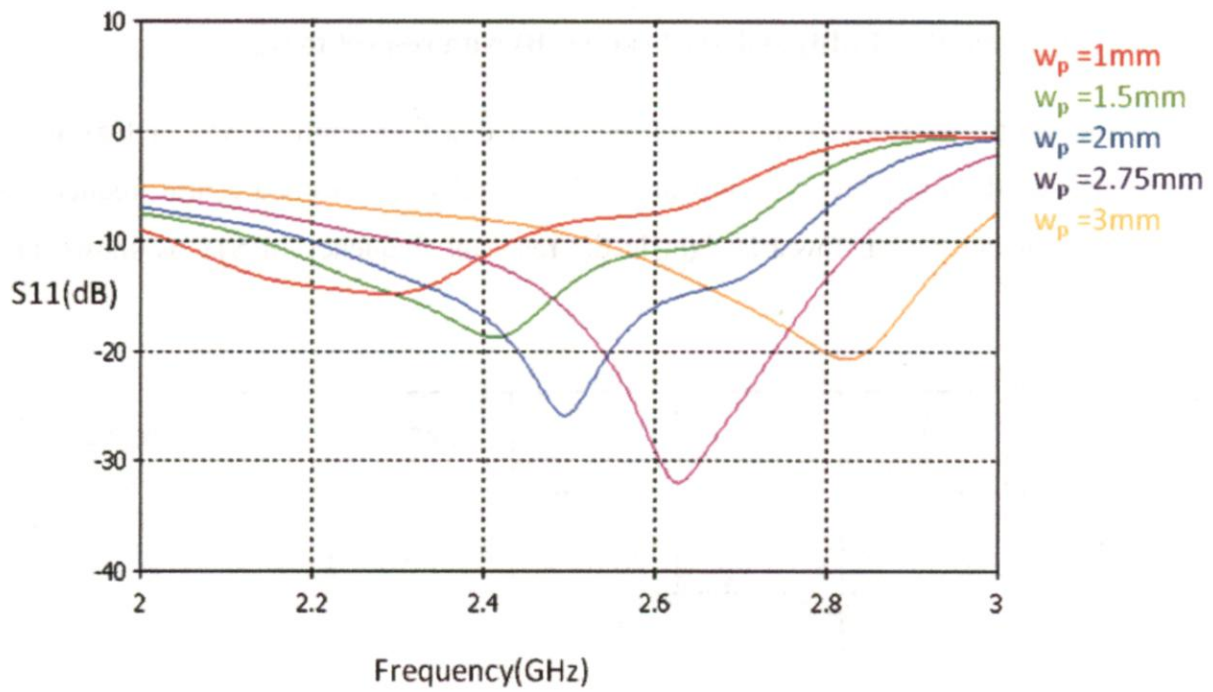
Figure 3.2 Variation of (a) axial ratio and (b) S11 with l_p

3.1.2.2 Variation of S11 (dB) and axial ratio (dB) with respect to w_p

Once the optimized value of l_p is obtained w_p is tuned to improve S11 and axial ratio. Increasing w_p does not have a significant effect on axial ratio around centre frequency but there is an apparent shift towards right in the resonant frequency of S11 as shown in the Figure 3.3.



(a)

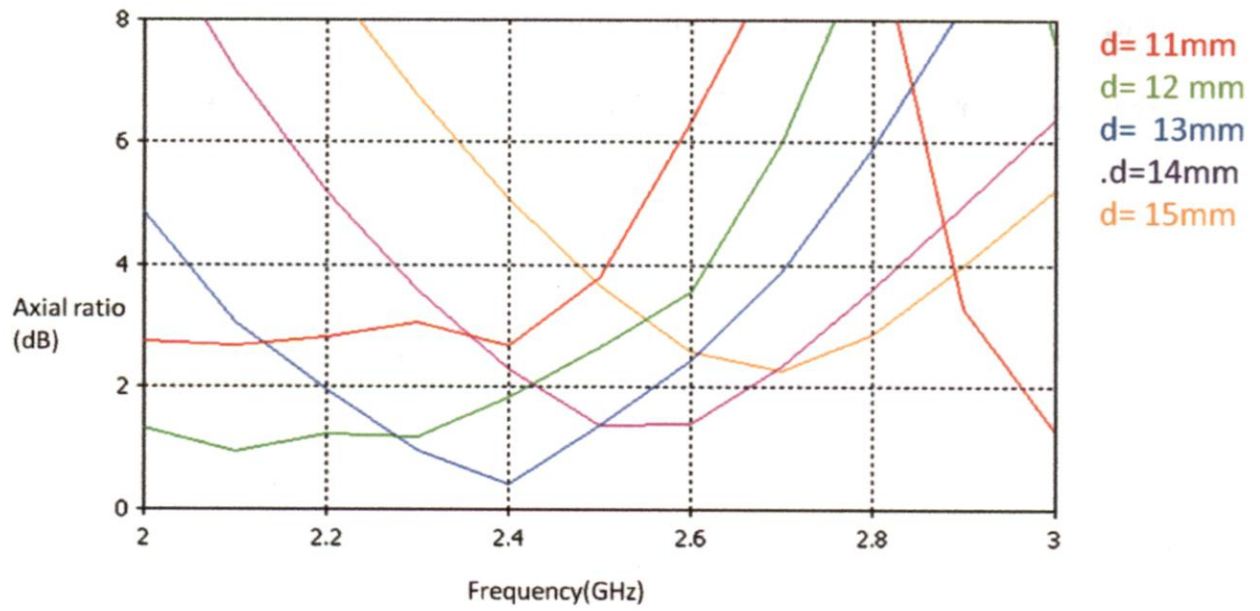


(b)

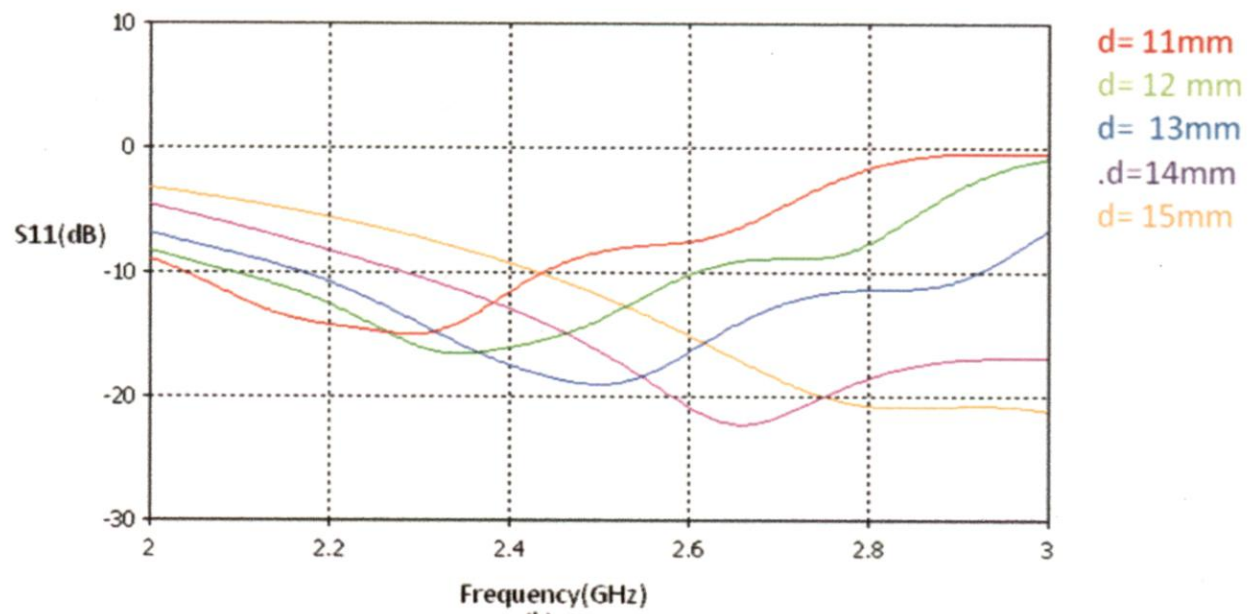
Figure 3.3 Variation of (a)axial ratio and (b)S11with w_p

3.1.2.3 Variation of S11 (dB) and axial ratio (dB) with respect to d

By varying the dimension of the slot cut on L shape feed line we have managed to get good S11, but axial ratio still needs improvement. This can be achieved by varying the slot size [Fig 3.4] of the annular slot.



(a)

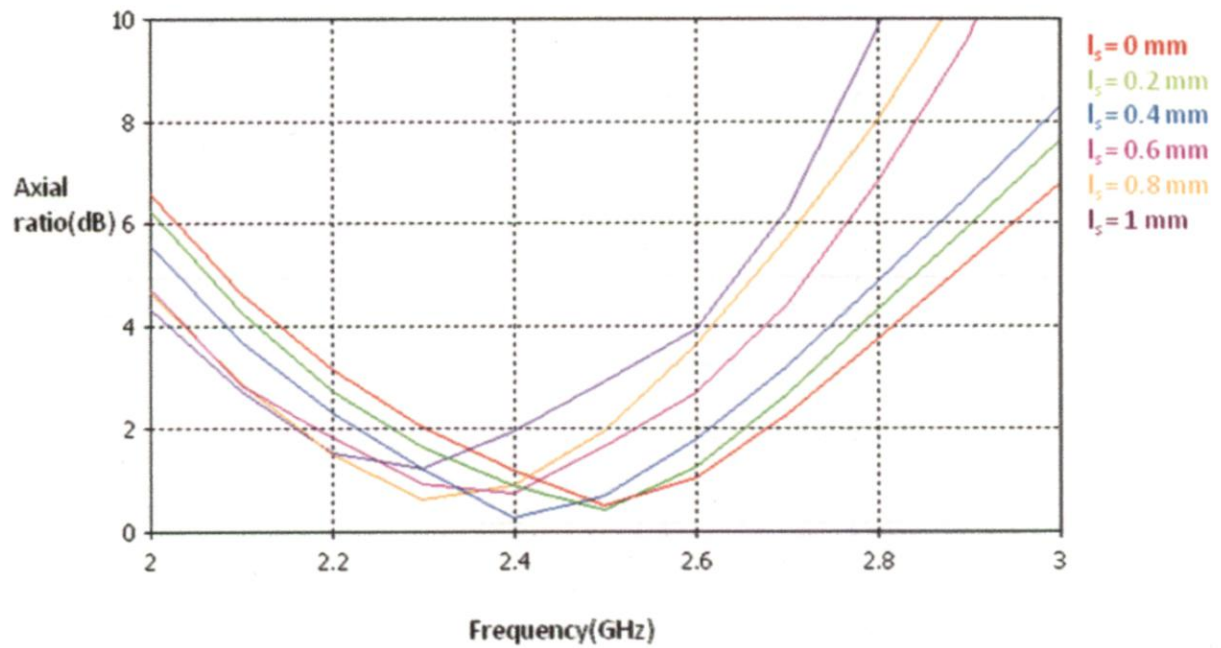


(b)

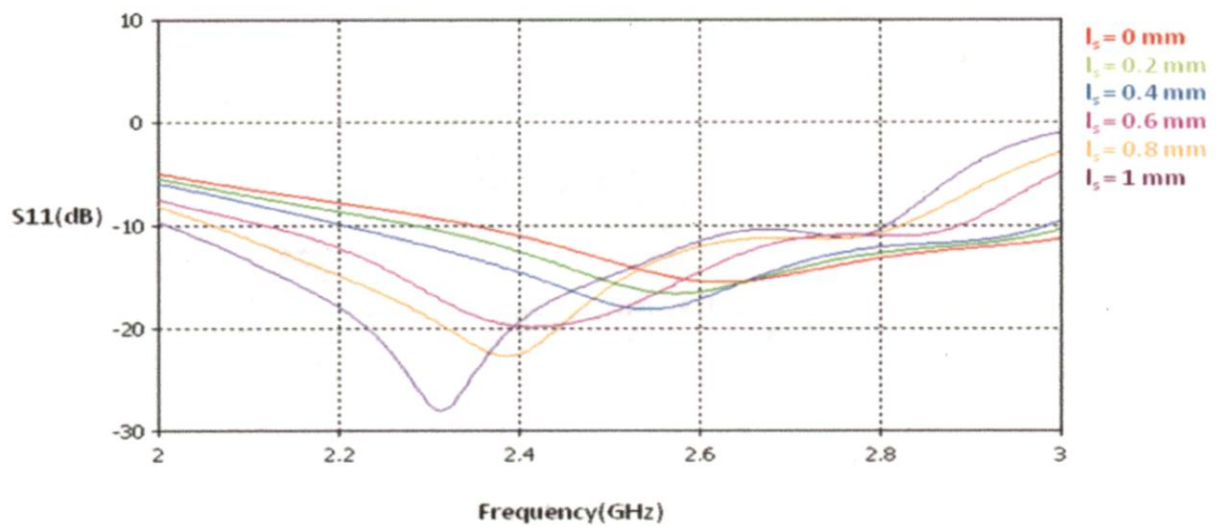
Figure 3.4 Variation of (a)axial ratio and (b)S11 with d

3.1.2.4 Variation of S11 (dB) and axial ratio (dB) with respect to l_s

The open circuit stub of length l_s is fine tuned to improve axial ratio and S11.



(a)



(b)

Figure 3.5 Variation of S11 and axial ratio with l_s

Table 3.2 Geometrical parameters of optimized antenna

Parameters	L_G	R_1	R_2	w_p	l_s	l_p	w	d	t
Dimension(mm)	50	19	6.5	2	0.6	15	4	12.5	10

Simulated results of the optimized antenna

The optimized values of the antenna parameter are presented in Table 3.2. Optimized results are given below.

3.2.1 S11 vs. Frequency

The plot between S11 and frequency is give in Figure 3.6.The figure shows that a bandwidth, for which $S_{11} < -10\text{dB}$, of around 32% about centre frequency 2.4 GHz is obtained.

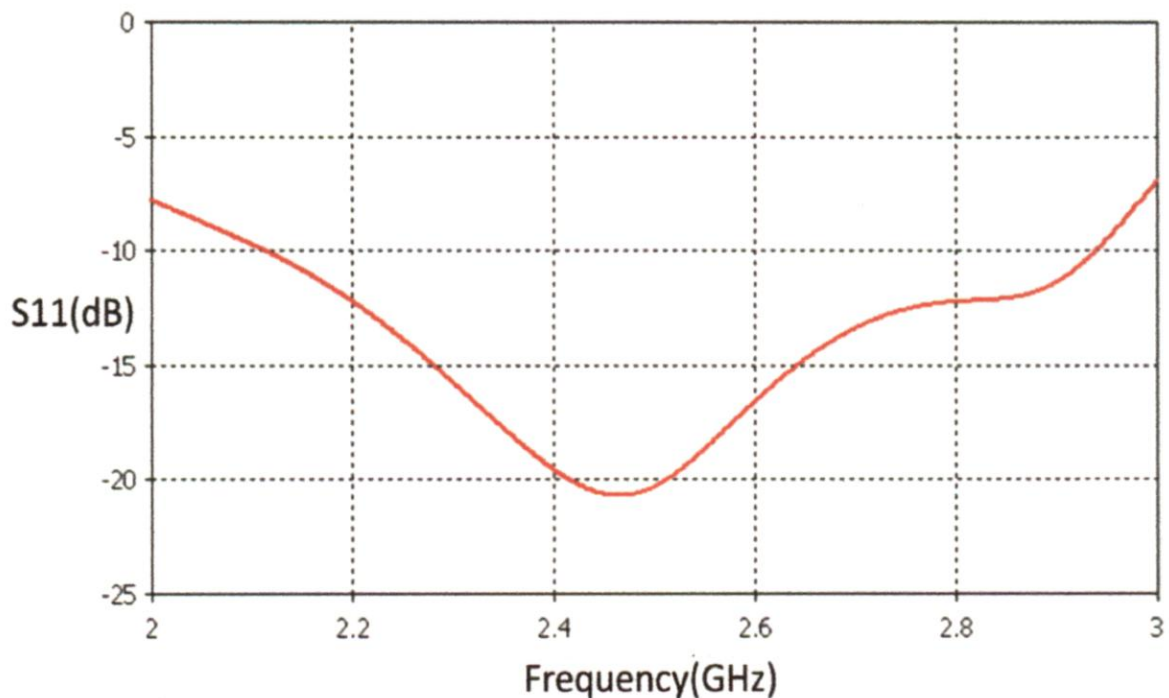


Figure 3.6 S11 vs. Frequency

3.2.2 Axial ratio vs. Frequency

The plot in Figure 3.7 shows the variation of axial ratio with frequency. The plot shows the axial ratio bandwidth, for which axial ratio $< 3\text{dB}$, of 14% around centre frequency 2.4 GHz.

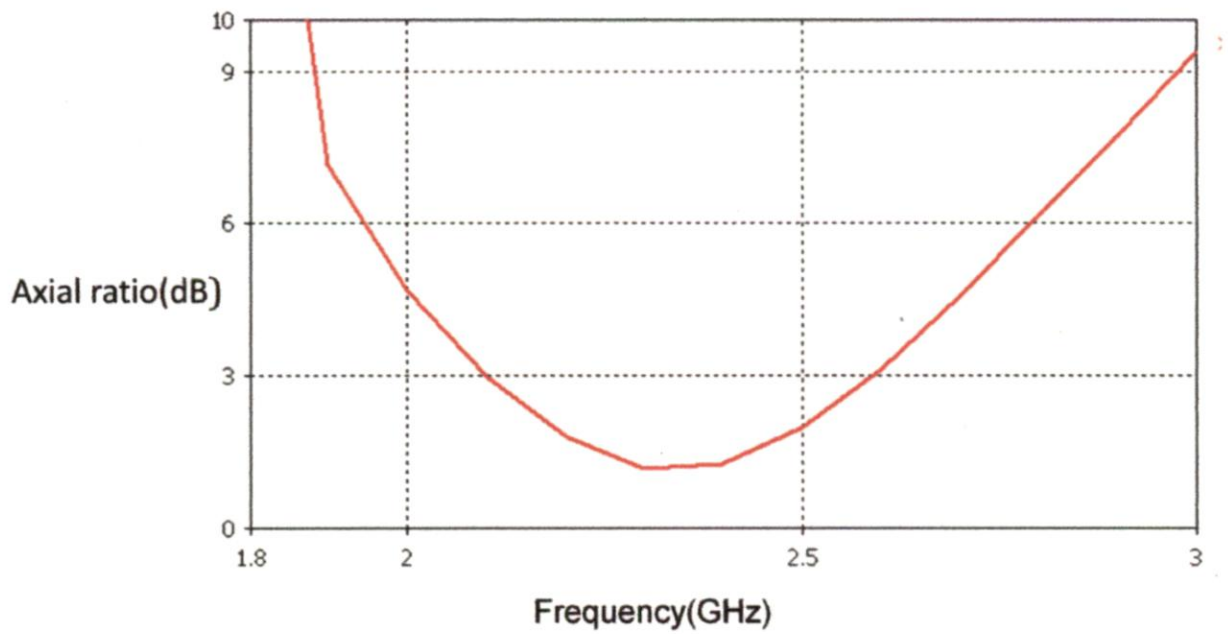


Figure 3.7 Axial ratio vs. Frequency

3.2.3 Gain vs. frequency

Figure 3.8 shows that a constant gain of is obtained in the desired frequency band 3.5 dB.

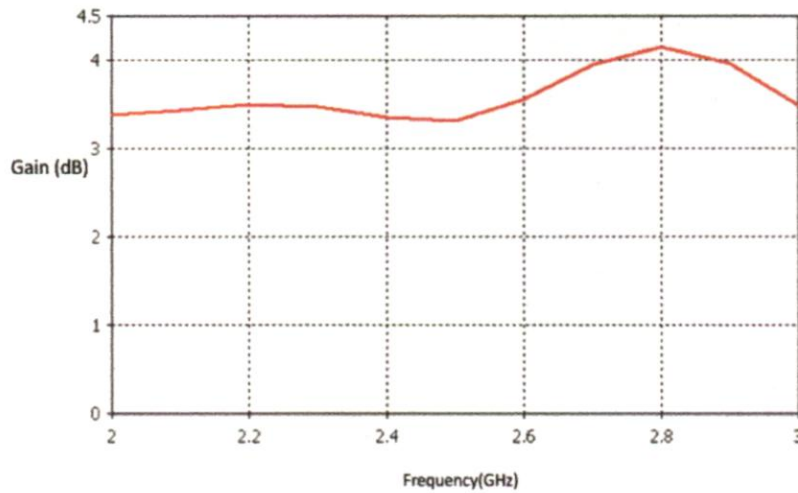


Figure 3.8 Gain vs. Frequency

3.2.4 Discussion of simulated results.

Simulated results of the optimized antenna are given in Figure 3.6, Figure 3.7 and Figure 3.8. Impedance bandwidth and axial ratio bandwidth have an overlapping region ($S_{11} < 10\text{dB}$ and axial ratio $< 3\text{dB}$) of 14%, in this region there is a constant gain of about 3.5dB.

Experimental set up for measurement

Measurement of S11 is carried out in vector network analyzer (VNA) as shown in the Figure 3.9



Figure 3.9 Measuring set up for S11

Measurement of axial ratio is carried out in anechoic chamber. The designed antenna is used as the receiving antenna and an S-band horn antenna is used as the transmitter. An arrangement is made as shown in the Figure 3.10. In this arrangement the antenna is posted on a wooden block with a hole, so that the antenna is free to move in the vertical plane about the line joining the centre of the horn and hole in the the wooden block. A polar plot is put behind the antenna and the angles from 0-340 are marked on it. To make the arrangement stable proper packing is given to the hole in the wooden block. The antenna is moved manually and readings are taken at the angles with 10^0 separations through a sensor which is connected to the antenna. The difference of the maximum and the minimum power received gives the axial ratio. The gain measurement has also been carried out in anechoic chamber using the same arrangement as used for measurement of axial ratio. For the measurement of the gain of a circularly polarized antenna, gain is measured for the vertical and the horizontal

position of the antenna. If the gain of antenna is G_V in vertical position and G_H in horizontal position then the net gain of the circularly polarized antenna is given by G_c [27]

$$G_c = 10 \log (G_V + G_H)$$

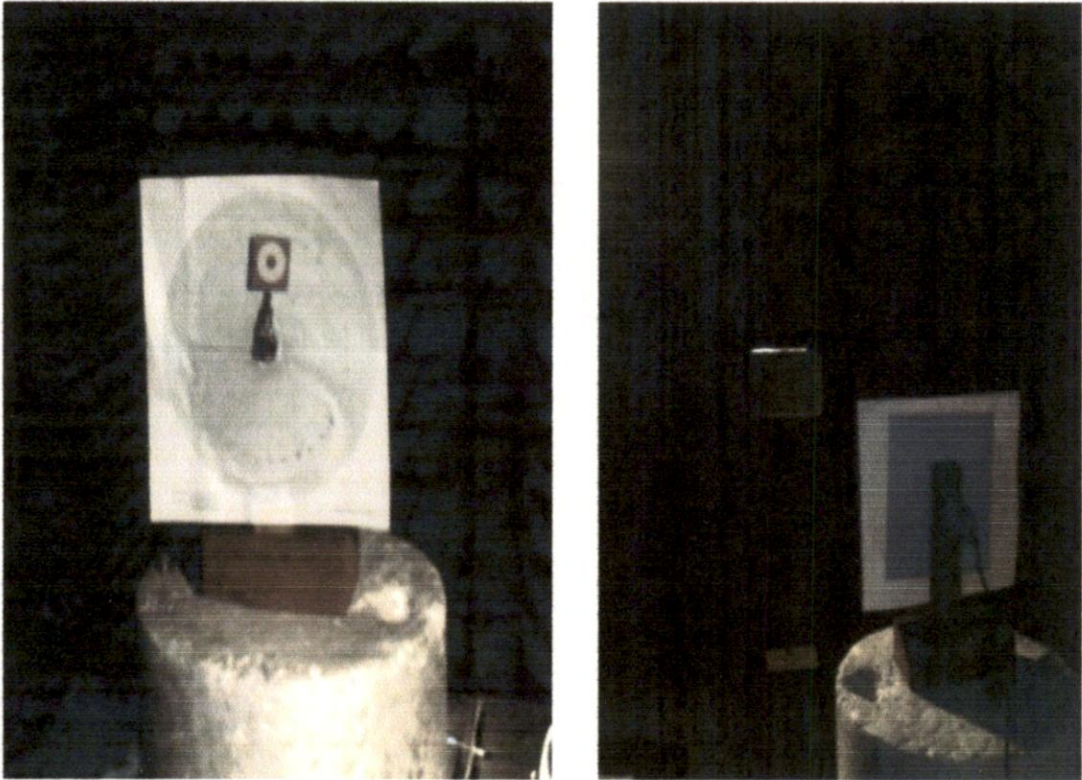


Figure 3.10 Set up for the measurement of axial ratio and gain

3.4 Measured results

3.4.1 Axial ratio vs. Frequency

Figure 3.11 shows the plot between axial ratio and frequency. The axial ratio bandwidth of 13% is obtained.

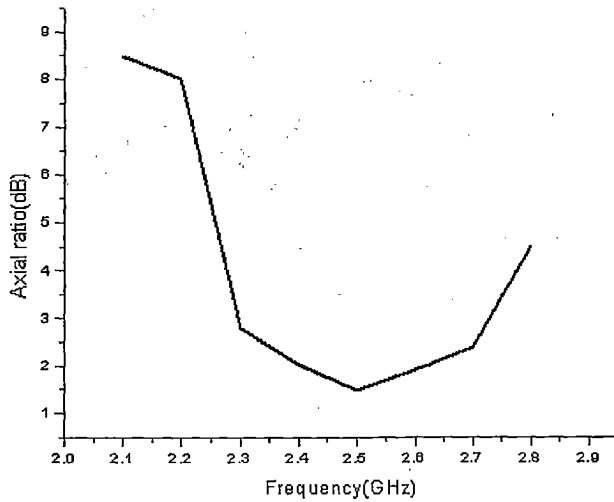


Figure 3.11 Axial ratio vs. Frequency

3.4.2 S11 vs. Frequency

Figure 3.12 shows the variation of S11 with frequency. The impedance bandwidth of 21% is obtained.

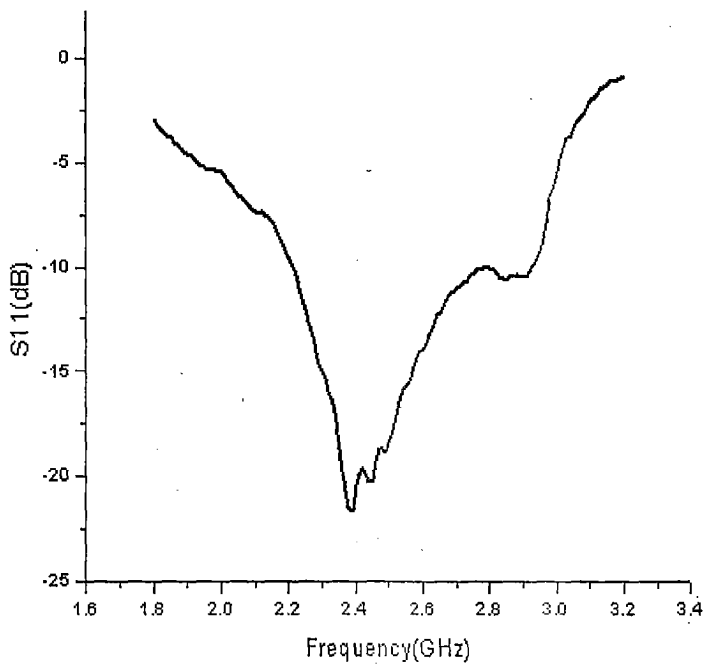


Figure 3.12 S11 vs. Frequency

3.4.3 Gain vs. Frequency

Figure 3.13 gives the plot between gain and frequency. The gain of 3.623dB is obtained at the centre frequency 2.4 GHz

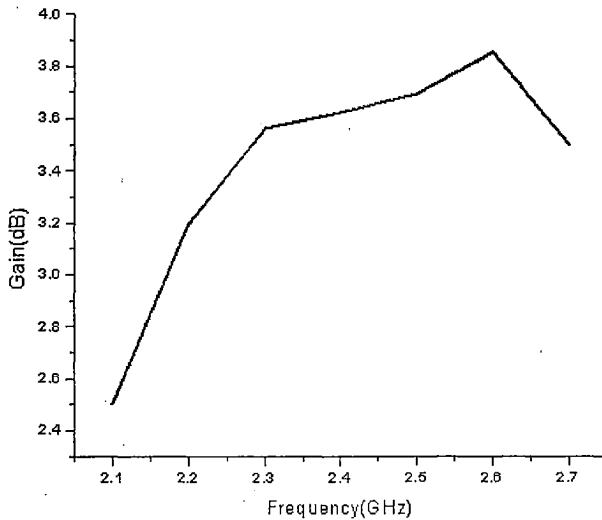


Figure 3.13 Gain vs. Frequency

Table 3.3 Gain vs. Frequency

Frequency(GHz)	Gain (dB)
2.1	2.5
2.2	3.2
2.3	3.56

2.4	3.623
2.5	3.693
2.6	3.85
2.7	3.5
2.8	3.2

Discussion of measured results

Measured results of the designed antenna are given in Figure 3.11 Figure 3.12 and Figure 3.13. Impedance bandwidth and axial ratio bandwidth have an overlapping region ($S_{11} < -10\text{dB}$ and axial ratio $< 3\text{dB}$) of 13%, in this region there is a constant gain of about 3.5dB

CHAPTER 4 Complementary Split Ring Resonators

This chapter contains the modeling of complementary split ring resonator (CSRR), simulated and measured results

4.1 Modeling of CSRR structure

CSRR structures are to be modelled so that their band stop frequency region falls in the operating frequency region of the antenna discussed in 3.1.

CSRR structures are modelled by the following procedure.

A 50 ohms microstrip line with an array CSRR etched on the ground plane is used. The CSRR is designed on a substrate of dielectric constant 3.2 having a thickness 1.5mm and is shown in Figure 4.1 and 4.2.

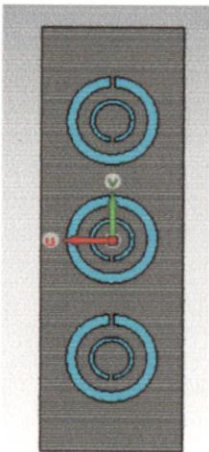


Figure 4.1 Top view

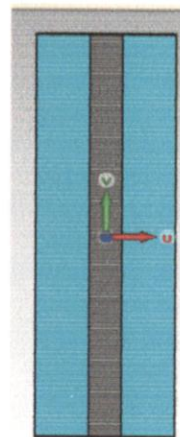
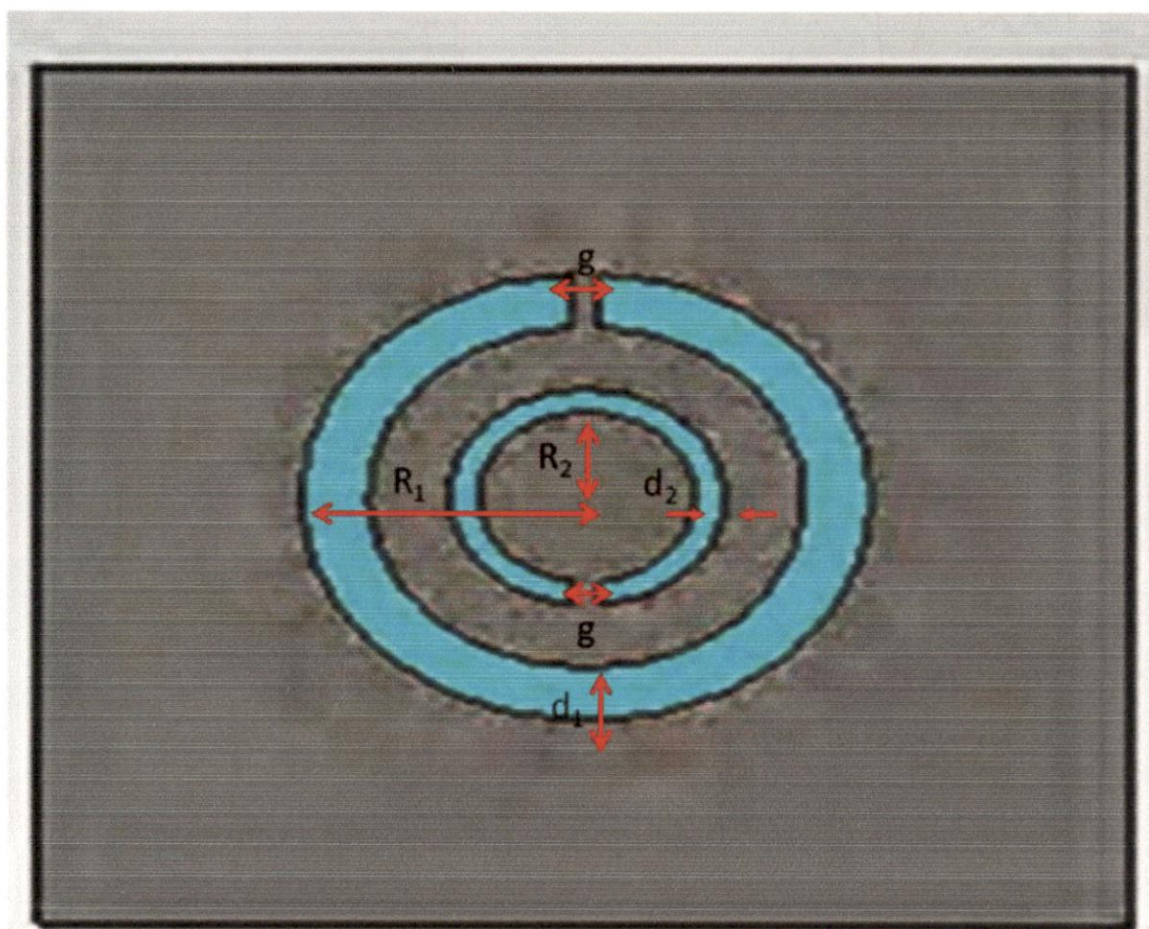


Figure 4.2 Bottom view

A single CSRR structure (Figure 4.3) has dimensions given in Table 4.1

Table 4.1 Geometrical parameters of a single CSRR structure

Parameter	R_1	R_2	d_1	d_2	g
Dimension(mm)	5.2	2.5	1.2	0.5	0.5



4.1.1 Simulated results of CSRR with microstrip line

The array of CSRR with microstrip line as shown in Figure 4.1 is simulated in CST Microwave Studio. From Figure 4.4 and 4.5 it is quite apparent that CSRR structures used here provide a wide stop band in the operational frequency region of the antenna. The wide band gap prohibits the propagation of surface waves and hence can be used as a reflecting surface for the antenna

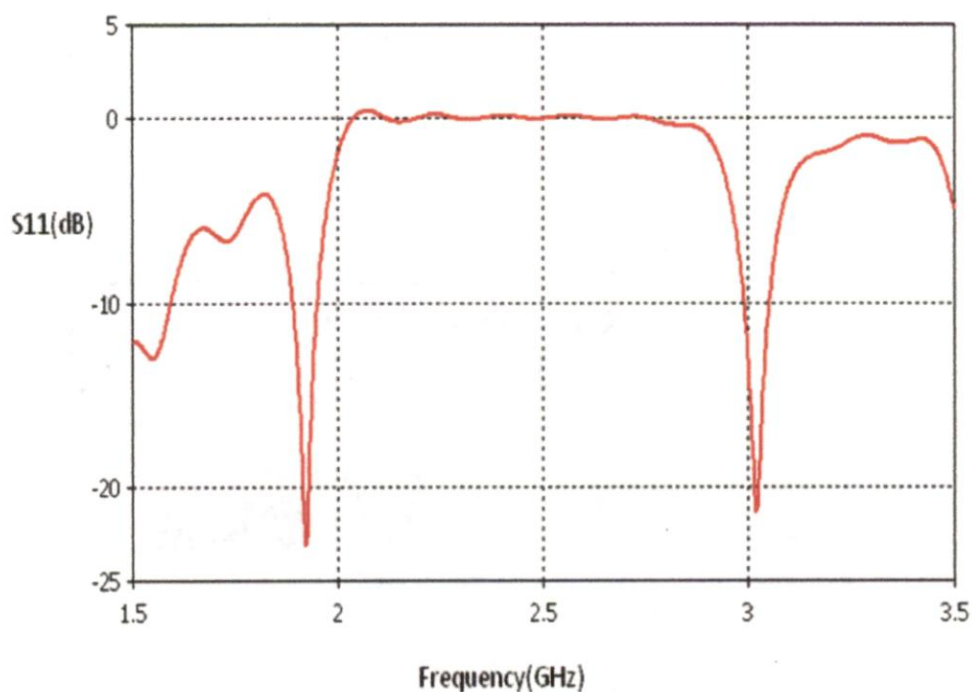


Figure 4.4 S11 (dB) vs. frequency

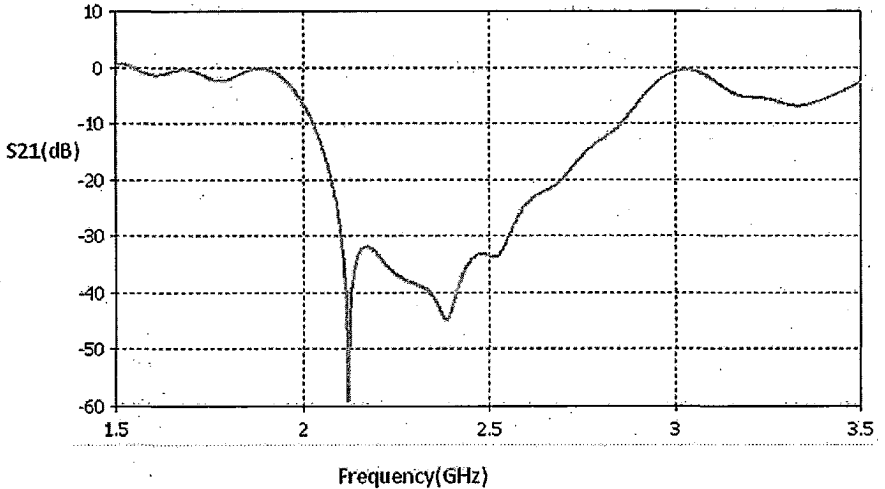


Figure 4.5 S21 (dB) vs. frequency

4.2 Effective electromagnetic parameters (ϵ, μ) of CSRR structure with microstrip line

To extract the effective electromagnetic parameters (ϵ, μ) Nicolson–Ross–Weir (NRW) approach [25] is used which is discussed in chapter 2.

In Figure 4.6 and 4.9 it is observed that real part of permittivity and imaginary part of permeability is negative respectively also Figure 4.7 and Figure 4.8 shows that the imaginary part of permittivity and imaginary part of permeability is positive in the operational frequency region which suggests that the structure modelled in 4.1 is a single negative metamaterial. In a single negative metamaterial only evanescent modes are present, thus waves cannot propagate in such a medium. Consequently if the CSRR are etched on a reflecting surface, they prohibit the propagation of surface waves.

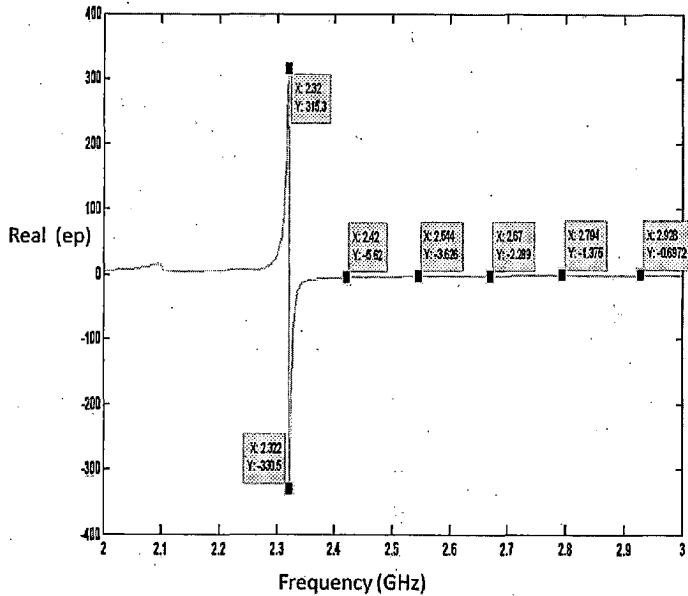


Figure 4.6 Real epsilon vs.Frequency

Table 4.2 Variation of real epsilon with frequency

Frequency (GHz)	Real epsilon
2.322	-330
2.42	-5.62
2.54	-3.626
2.67	-2.289
2.794	-1.375
2.928	-0.692

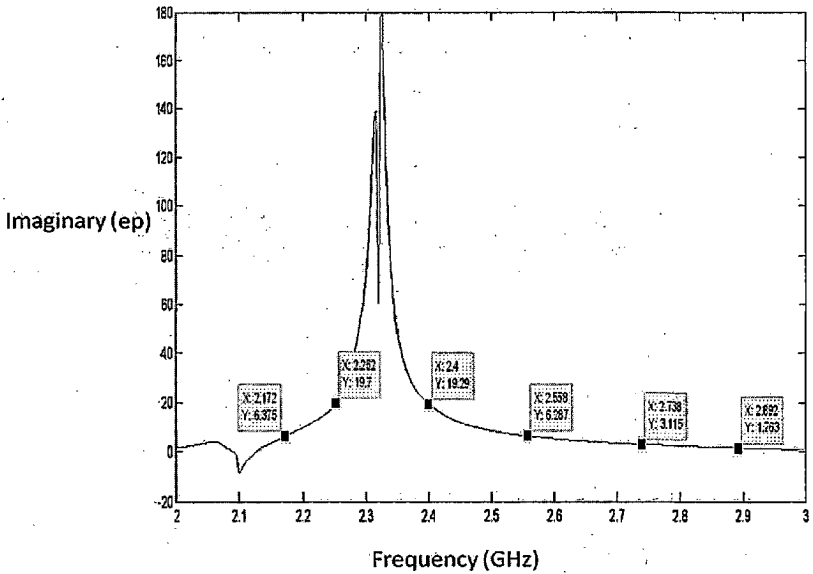


Figure 4.7 Imaginary epsilon vs. frequency

Table 4.3 Variation of Imag (ep) with frequency

Frequency (GHz)	Imaginary epsilon
2.172	6.375
2.252	19.7
2.4	19.29
2.558	6.287
2.738	3.115
2.8892	1.763

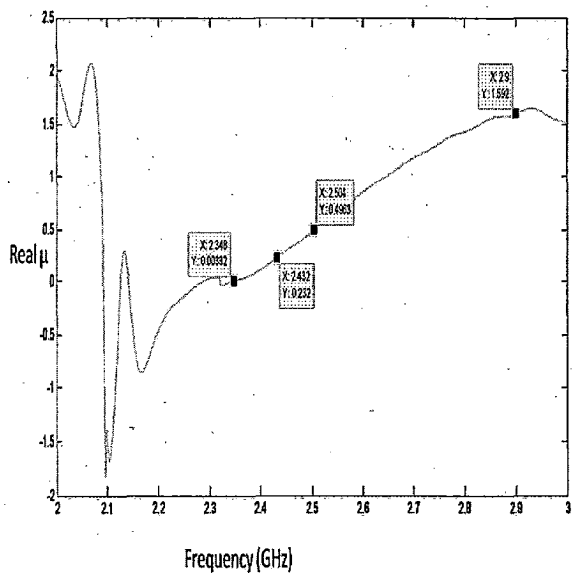


Figure 4.8 Real (μ) vs. Frequency

Table 4.4 Variation of Real (μ) with frequency

Frequency(GHz)	Real μ
2.348	0.00332
2.432	0.232
2.504	0.4963
2.9	1.592

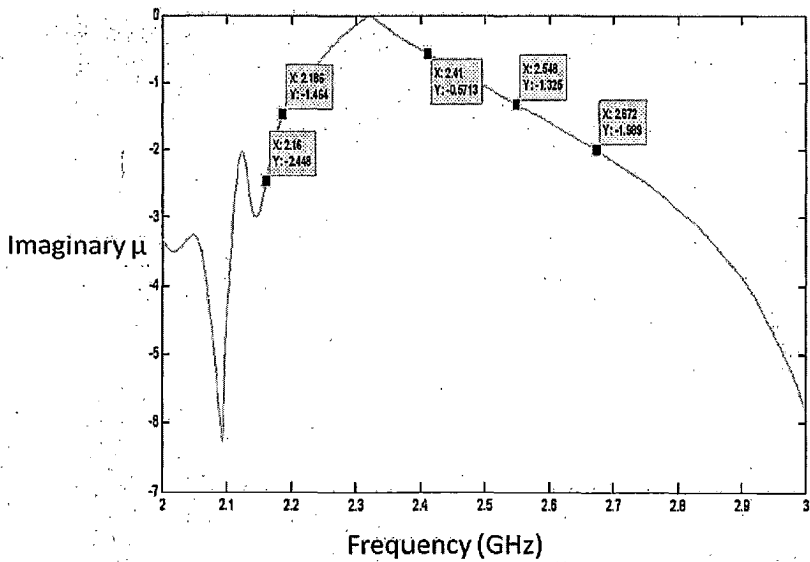


Figure 4.9 Imaginary μ vs. Frequency

Table 4.5 Variation of Imag (μ) with frequency

Frequency (GHz)	Imaginary μ
2.15	-2.448
2.186	-1.464
2.41	-0.5123
2.548	-1.325
2.672	-1.99

4.3 Equivalent circuit model of the CSRR structure with microstrip line

This equivalent circuit model of CSRR with microstrip line consists of a three-element LC tank circuit. The shunt LC tank circuit includes a series LC resonator (L and C_1) and a capacitance element (C_2) connected in parallel (Figure 4.10). From Figure 4.4 and 4.5 we can obtain frequency f_1 , f_2 and f_3 as discussed in chapter 2. In the equivalent circuit model, there are two characteristic frequencies f_1 and f_2 . f_1 is given by the resonance condition of the whole tank circuit, which leads to the zeros of the reflection coefficient (S_{11}). f_2 is given by the resonance condition of the series LC circuits (L and C_1), which leads to the zeros of the transmission coefficient (S_{21}). These frequencies are given by the following expressions

$$f_1 = 1/2\pi \sqrt{\frac{C_1 + C_2}{LC_1 C_2}}$$

$$f_2 = 1/2\pi \sqrt{\frac{1}{LC_1}}$$

Using the following equations we can obtain the equivalent circuit model

$$C_2 = \frac{Y_0(f_2^2 - f_1^2)}{\pi f_2(f_1^2 - f_2^2)}$$

$$C_1 = \left(\frac{f_1^2}{f_2^2} - 1\right) C_2$$

$$L = \frac{1}{4\pi^2 f_2^2 C_1}$$

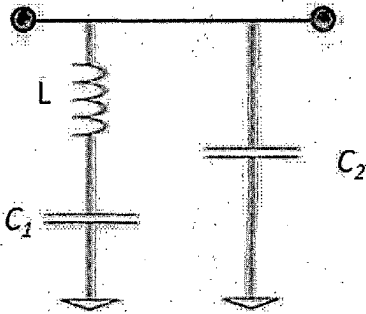


Figure 4.10 Equivalent circuit model of microstrip loaded with CSRR structure

Table 4.6 Parameters and values of equivalent circuit of CSRR with microstrip line

Parameter	f_1	f_2	f_3	c_1	c_2	L
Values	2.008 GHz	2.4 GHz	2.075 GHz	0.19pF	-3pF	0.23nH.

4.4 Measured permittivity and permeability

To measure the complex permittivity and permeability, a 50 ohm microstrip line with an array CSRR etched on the ground plane is used as shown in the Figure 4.1 and 4.2. S_{11} and S_{21} are measured in polar form (amplitude and angle), after that Nicolson–Ross–Weir (NRW) approach is followed, to get complex permittivity and permeability.

Figure 4.11 shows the complex permittivity whereas Figure 4.12 shows complex permeability. The measured results are in good agreement with the simulated ones.

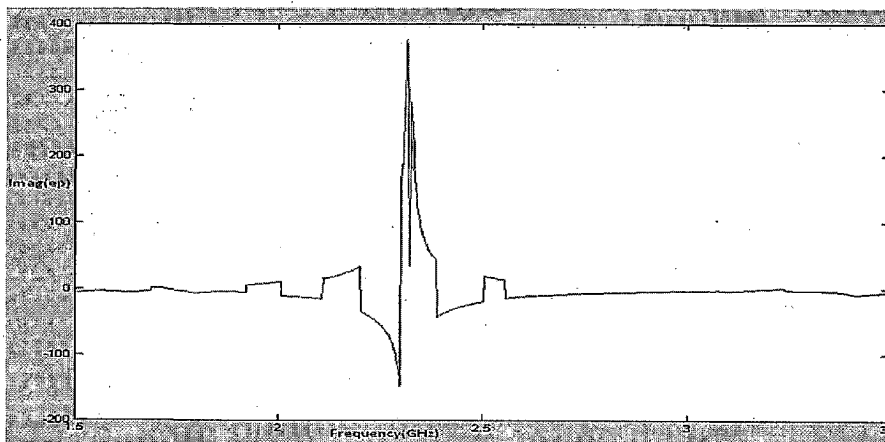
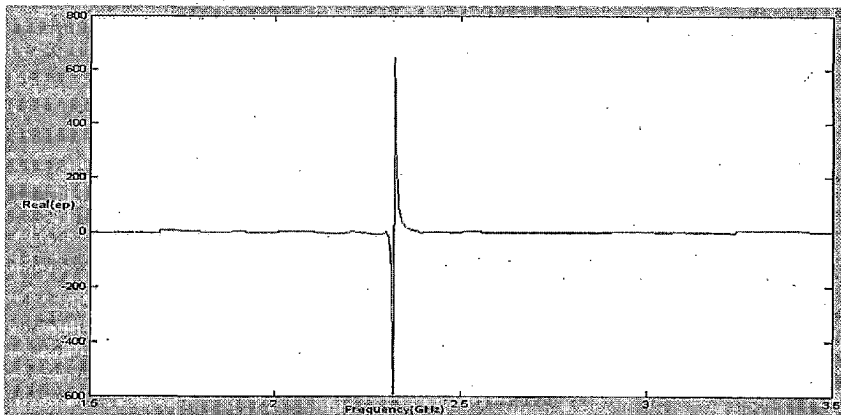


Figure 4.11 Complex permittivity vs. Frequency

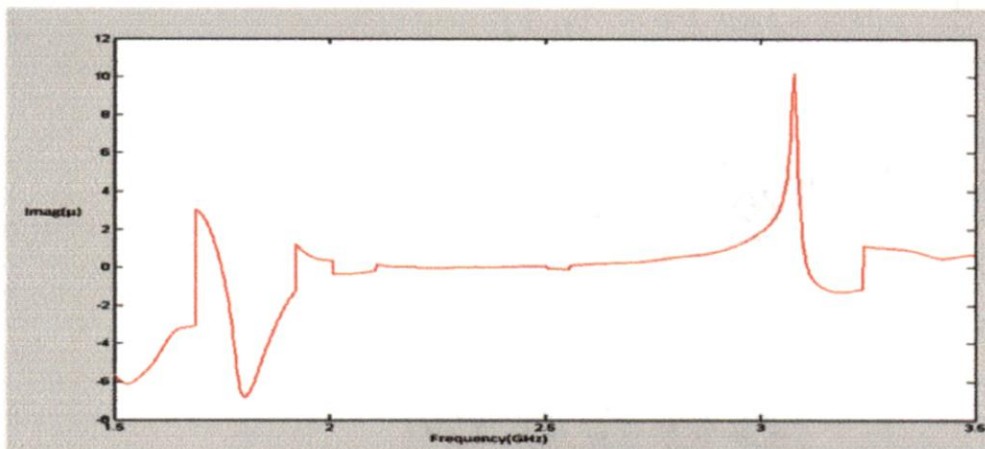
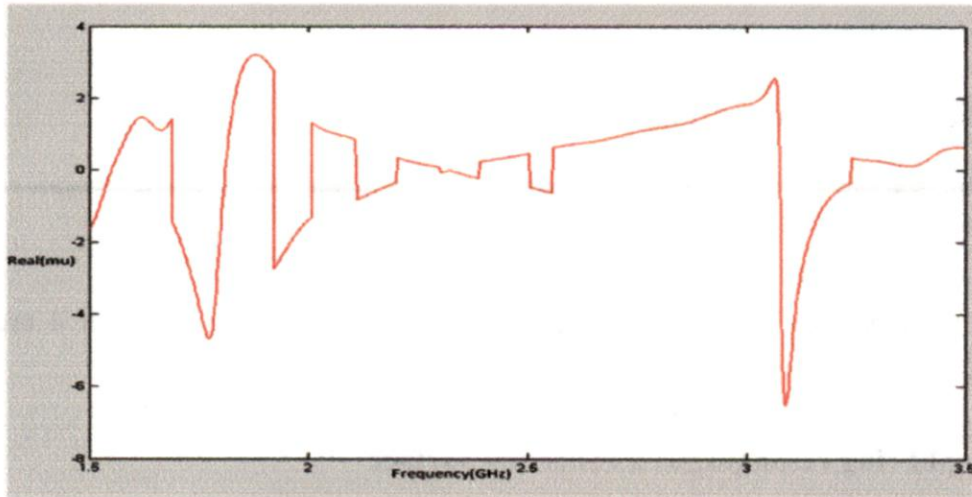


Figure 4.12 Complex permeability vs. Frequency

CHAPTER 5

Antenna with CSRR reflecting surface

In this chapter the complementary split ring resonators (CSRR) modelled in chapter 4 are used with the optimized antenna of chapter 3.

5.1 Complementary split ring resonator as a reflecting surface

Complementary split ring resonators are etched on a substrate of dielectric constant 3.2 as shown in the Figure 5.1

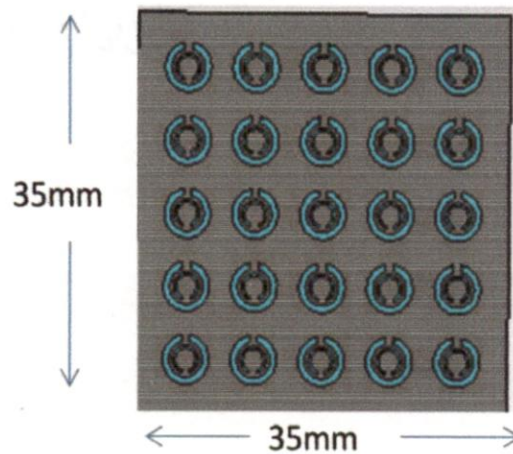


Figure 5.1 CSRR reflector

Figure 5.2 shows the antenna with CSRR reflector. The reflector is kept 19 mm below the antenna. With a PEC reflector this distance should be at least $\lambda_0/4$ (31mm) at centre frequency 2.4 GHz. Thus by using CSRR reflector we manage to reduce the distance between antenna and reflector thus low profiling of antenna is done.

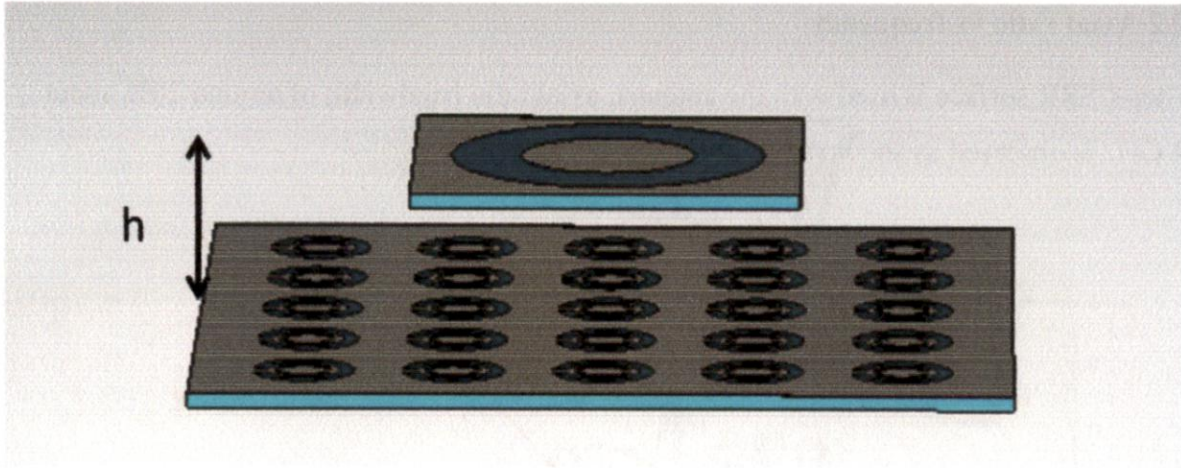


Figure 5.2 Reflector h distance below the antenna

5.2 Simulated results of the antenna with reflector

5.2.1 S11 vs. Frequency

When CSRR surface is used with the antenna, impedance bandwidth of 45% around 2.4 GHz is observed as shown in the Figure 5.3

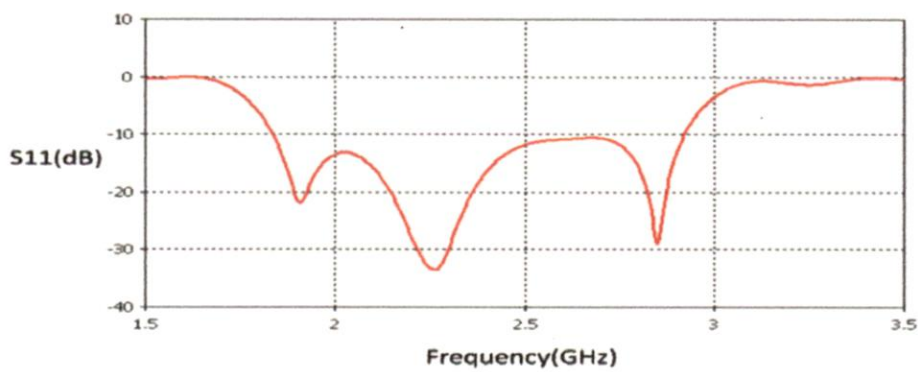


Figure 5.3 S11 Vs frequency

5.2.2 Axial ratio vs frequency

When CSRR surface is used with the antenna, axial ratio bandwidth of around 20% about 2.4 GHz is observed as shown in the Figure 5.4

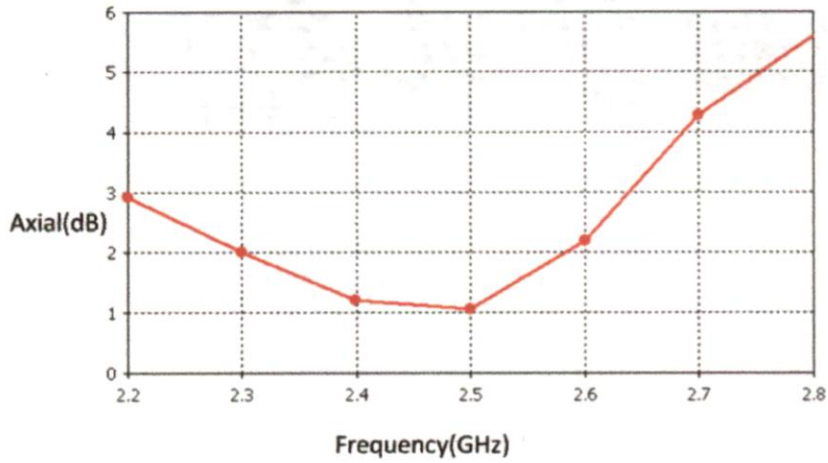
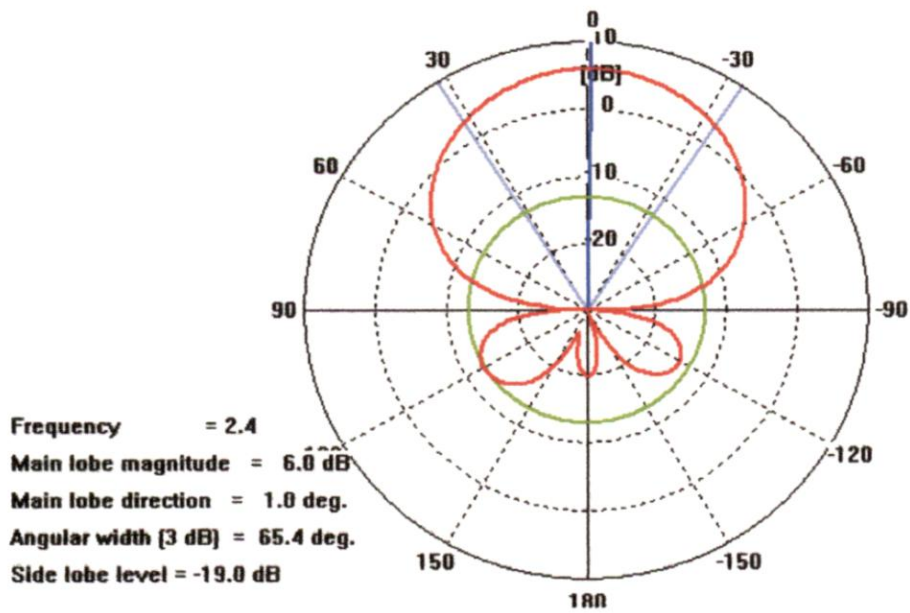


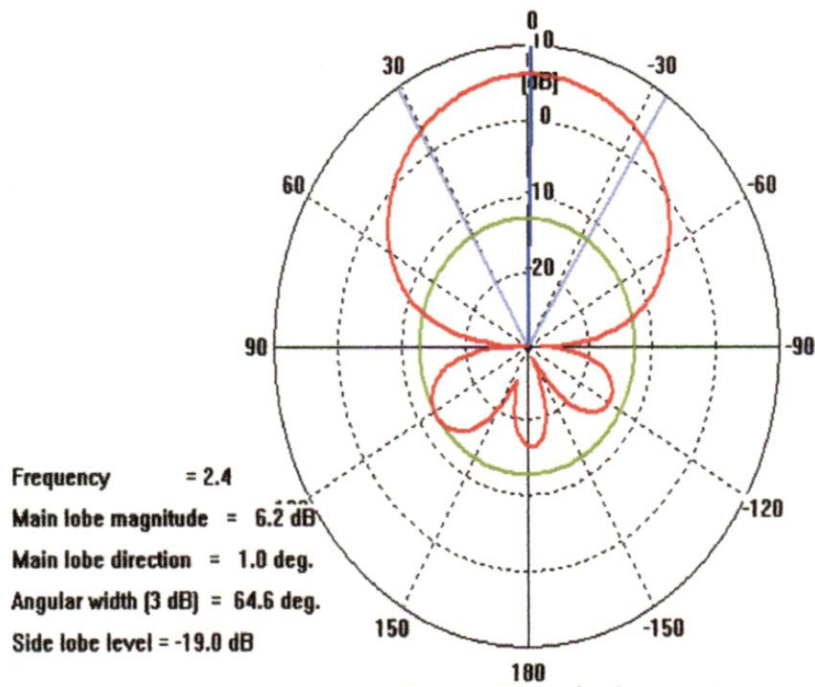
Figure 5.4 Axial ratio Vs frequency

5.2.3 Radiation pattern

A unidirectional radiation pattern is observed as shown in the Figure 5.5. The radiation pattern of a slot antenna is bidirectional, CSRR reflecting surface makes this pattern unidirectional



(a) Radiation pattern in X-Z plane



(b) Radiation pattern in Y-Z plane

Figure 5.5 Radiation pattern (a) X-Z (b) Y-Z

5.2 Discussion of measured results

Measured results are given in Figure 5.6, Figure 5.7, and Figure 5.8. Impedance bandwidth and axial ratio bandwidth have an overlapping region ($S_{11} < -10\text{dB}$ and axial ratio $< 3\text{dB}$) of 20%. Figure 5.8 shows that antenna has a unidirectional radiation pattern.

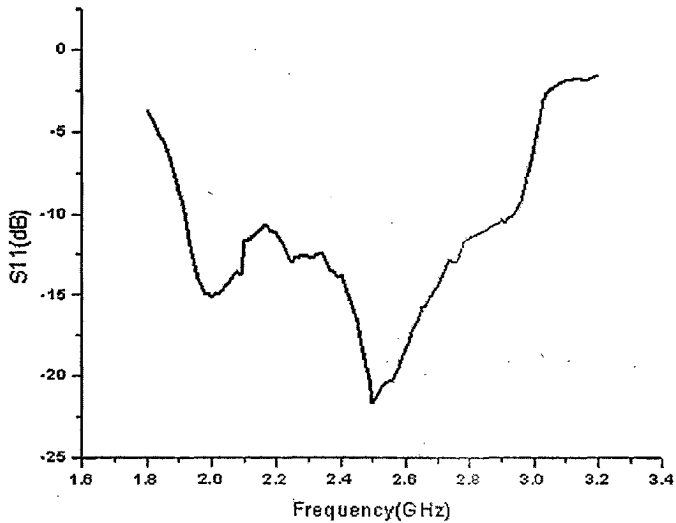


Figure 5.6 S11 Vs Frequency

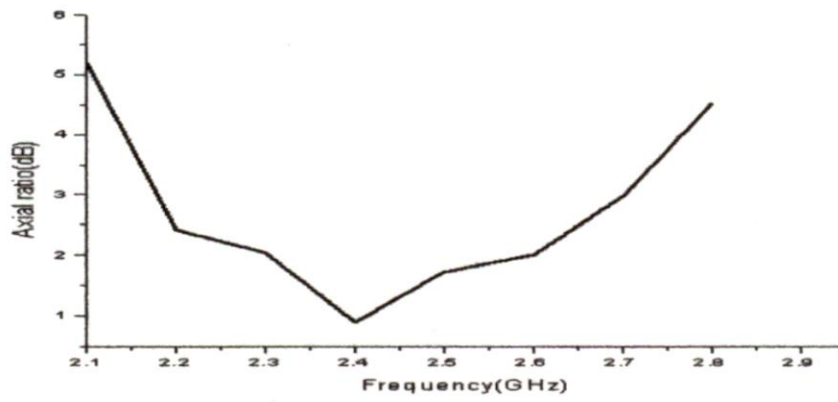
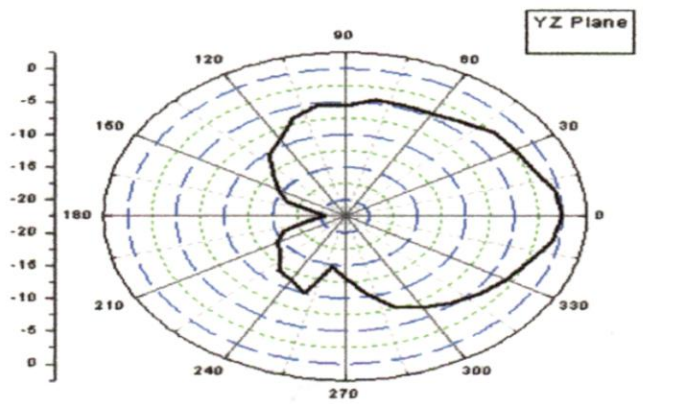
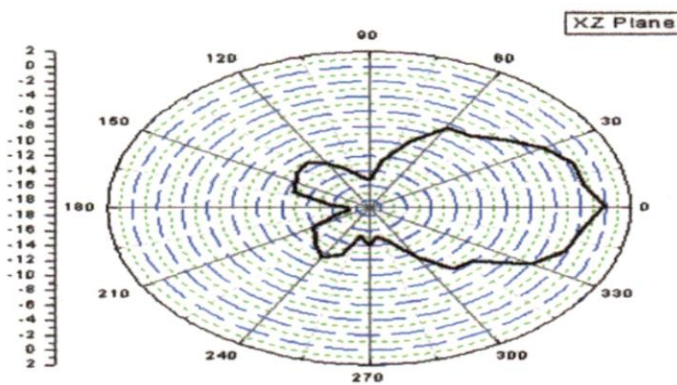


Figure 5.7 Axial ratio Vs frequency



(a)



(b)

Figure 5.8 Radiation pattern (a) Y-Z (b) X-Z

CHAPTER 6

Conclusion and future scope

A circularly polarized slot antenna is designed. The slot has annular ring geometry. The slot is fed by L shape feed line which couples two orthogonal side of the ring to provide circular polarization. Since the antenna is meant for broad band application, a wide ring slot is used. The antenna is optimized in CST microwave studio by varying different parameters of the antenna. The optimized antenna is fabricated and its performance is observed by measuring S11, axial ratio and gain.

Measured results show that the antenna has the impedance bandwidth of 21% and the axial ratio bandwidth of 13%. The antenna has an overlapping region ($S_{11} < -10\text{dB}$ and axial ratio $< 3\text{dB}$), in this region there is a constant gain of 3.5dB with bidirectional radiation pattern. To make the radiation pattern unidirectional and to enhance the performance of antenna complementary split ring structures are used. An array of CSSR structures are etched on the substrate of dielectric constant 3.2.

This surface is used as a reflector. CSRR structures are modeled such that their band stop frequency region falls in the operating frequency region of the antenna. This surface suppresses surface waves and makes the radiation pattern unidirectional.

Measured results of antenna with CSRR reflecting surface shows that the antenna has a unidirectional radiation pattern with impedance bandwidth of 45% and axial ratio bandwidth of 20% about 2.4GHz. The antenna has an overlapping region ($S_{11} < -10\text{dB}$ and axial ratio $< 3\text{dB}$) of 20%.

The distance between the CSSR reflecting surface and the antenna is 19mm. When perfectly electric conductor (PEC) reflector is used this distance should be at least $\lambda/4$ (31mm at 2.4 GHz) which increases the vortical profile of the antenna. Thus by using CSRR reflecting surface low profiling is achieved.

Future scope

The distance between the reflecting plane and the antenna can further be reduced by rigorous optimization of antenna.

The antenna reported in this dissertation is right hand circularly polarized if the orientation of the L shape feed line is changed left hand circularly polarization is obtained. Because of this feature of the antenna , polarization diversity between left-hand circular polarization (LHCP) and right-hand circular polarization (RHCP) can be obtained using a T shape feed line with switching diodes.

REFERENCES

- [1] Moini, R., M. Samiee, A. Tavakoli, and G. Z. Rafi, "A dual-feed dual- excitation mode circularly-polarized crossed-slot antenna," *IEEE Antennas and Propagat. Soc. Int. Symp. Dig.*, Vol. 2, 58–61, Jul. 1996
- [2] Nestic, A. and S. Jovanovic, "New printed slot antenna with circular polarization ," *IEEE Antennas and Propagat. Soc. Int. Symp. Dig.*, Vol. 3, 1870–1873, Jul. 1997
- [3] Shen, Z., C. T. Sze, and C. L. Law, "A circularly polarized Microstrip-fed T-slot antenna," *IEEE Antennas and Propagat. Soc. Int. Symp. Dig.*, Vol. 2, 1008–1010, Jul. 2000
- [4] Wong, K. L., C. C. Huang, and W. S. Chen, "Printed ring slot antenna for circular polarization," *IEEE Trans. Antennas and Propagat.*, Vol. 50, 75–77, Jan. 2002.
- [5] Sze, J. Y., K. L. Wong, and C. C. Huang, "Coplanar waveguide-fed square slot antenna for broadband circularly polarized radiation," *IEEE Trans. Antennas and Propagat.*, Vol. 51, 2141–2144, Aug. 2003
- [6] Qing, X. M. and Y. W. M. Chia, "Circularly polarized circular ring slot antenna fed by stripline hybrid coupler," *Electron. Lett.*, Vol. 35, 2154–2155, Dec. 1999
- [7] Qing, X. M. and Y. W. M. Chia, "Broadband circularly polarized slot loop antenna fed by three stub hybrid coupler," *Electron. Lett.*, Vol. 35, 1210–1211, Jul. 1999
- [8] Row, J. S., "The design of a squarer-ring slot antenna for circular polarization," *IEEE Trans. Antennas and Propagat.*, Vol. 53, 1967–1972, Jun. 2005
- [9] F. R. Yang, R. Coccioli, Y. Qian, and T. Itoh, "Planar PBG structures: Basic properties and applications," *IEICE Trans. Electron.*, vol. E83-C, no. 5, pp. 87–696, May 2000

- [10] C. Caloz and T. Itoh, "Multilayer and anisotropic planar compact PBG structures for microstrip applications," *IEEE Trans. Microwave Theory Tech.*, vol. 50, pp. 2206–2208, Sept. 2002
- [11] F. R. Yang, K. P. Ma, Y. Qian, and T. Itoh, "A uniplanar compact photonic-bandgap (UC-PBG) structure and its applications for microwave circuits," *IEEE Trans. Microwave Theory Tech.*, vol. 47, pp. 1509–1514, Aug. 1999.
- [12] C. Caloz and T. Itoh, "Multilayer and anisotropic planar compact PBG structures for microstrip applications," *IEEE Trans. Microwave Theory Tech.*, vol. 50, pp. 2206–2208, Sept. 2002
- [13] J. B. Pendry, A. J. Holden, D. J. Robbins, and J. Stewart, "Magnetism from conductors and enhanced nonlinear phenomena," *IEEE Trans. Microwave Theory Tech.*, vol. 47, pp. 2075–2084, Nov. 1999
- [14] D. R. Smith, W. J. Padilla, D. C. Vier, S. C. Nemat-Nasser, and S. Schultz, "Composite medium with simultaneously negative permeability and permittivity," *Phys. Rev. Lett.*, vol. 84, pp. 4184–4187, May 2000
- [15] F. Falcone, F. Martín, J. Bonache, J. Martel, R. Marqués, T. Lopetegi, M.A. G. Laso, and M. Sorolla, "Implementation of negative- μ structures in microstrip technology," in *Proc. 28th Int. Conf. Infrared Millimeter Waves (IRMMW'03)*, Shiga, Japan, Sept-Oct. 2003
- [16] R. Marqués, F. Mesa, J. Martel, and F. Medina, "Comparative analysis of edge and broadside-coupled split ring resonators for metamaterial design. Theory and experiments," *IEEE Trans. Antennas Propagat.*, vol. 51, pp. 2572–2581, Oct. 2003
- [17] Jackson, D. R. and N. G. Alexopoulos, "Gain enhancement methods for printed circuit antenna," *IEEE Transactions on Antennas and Propagation*, Vol. 33, 976-987, Sep. 1985.

- [18] Yang, H. Y. and N. G. Alexopoulos, "Gain enhancement methods for printed circuit antennas through multiple superstrates," *IEEE Transactions on Antennas and Propagation*, Vol. 35, No. 7, 860- 863, Jul. 1987.
- [19] Shen, X.-H., G. A. E. Vandenbosch, and A. R. Van de Capelle, "Study of gain enhancement method for microstrip antenna using moment method," *IEEE Transactions on Antennas and Propagation*, Vol. 43, No. 3, 227-231, Mar. 1995.
- [20] Lee, R. Q., K. F. Lee, and J. Bobinchak, "Characteristics of a two-layer electromagnetically coupled rectangular patch antenna," *Electronics Letters*, Vol. 23, No. 20, 1301-1302, 1987.
- [21] Nishiyama, E., M. Aikawa, and S. Egashira, "Stacked microstrip antenna for high-gain and wideband," *IEE Proc Microw. Antennas Propag.*, Vol. 151, No. 2, 143-48, Apr. 2004.
- [22] T. N. Chang, M. C. Wu, J.-M. Lin "Gain enhancement for circularly polarized microstrip patch antenna", *Progress In Electromagnetics Research B*, Vol. 17, 275-292, 2009
- [23] C. K. Kumar and S. N. Sinha "A patch loaded ring slot antenna for wide band circular polarization", *J. of Electromagn. Waves and Appl.*, Vol. 23, 2409-2419, 2009 .
- [24] C Li and Fang Li "Characterization and modeling of a microstrip line loaded with complementary split-ring resonators (CSRRs) and its application to high pass filters", *J. Phys. D: Appl. Phys.* Vol 40, (2007) 3780-3787
- [25] Shau-Gang Mao, Shiou-Li Chen and Chen-Wei Huang "Effective electromagnetic parameters of novel distributed left-handed microstrip lines", *IEEE Transactions on microwave theory and techniques*, VOL. 53, NO. 4, APRIL 2005
- [26] Aliakbar Dastranj, Ali Imani, and Mohammad Naser-Moghadassi, "Printed wide-slot antenna for wideband applications", *IEEE Transactions on Antennas and Propagation*, Vol. 56, No. 10, 227-231, Oct 2008.